Journal of
METAMORPHIC GEOLOGY

J. metamorphic Geol., 2013, **31,** 549–570 doi:10.1111/jmg.12033

Exhumation of oceanic eclogites: thermodynamic constraints on pressure, temperature, bulk composition and density

Y. CHEN, K. YE, T. F. WU AND S. GUO
State Key Laboratory of Lithospheric Evolution, Institute of Geology and Geophysics, Chinese Academy of Sciences, P.O. Box 9825, Beijing, 100029, China (chenyi@mail.iggcas.ac.cn)

ABSTRACT The exhumation mechanism of high-pressure (HP) and ultrahigh-pressure (UHP) eclogites formed by the subduction of oceanic crust (hereafter referred to as oceanic eclogites) is one of the primary uncertainties associated with the subduction factory. The phase relations and densities of eclogites with MORB compositions are modelled using thermodynamic calculations over a *P–T* range of 1–4 GPa and 400–800 °C, respectively, in the NCKFMASHTO (Na_2O–CaO–K_2O–FeO–MgO–Al_2O_3–SiO_2–H_2O–TiO_2–Fe_2O_3) system. Our modelling suggests that the mineral assemblages, mineral proportions and density of oceanic crust subducted along a cold *P–T* path are quite different from those of crust subducted along a warm *P–T* path, and that the density of oceanic eclogites is largely controlled by the stability of low-density hydrous minerals, such as lawsonite, chlorite, glaucophane and talc. Along a cold subduction *P–T* path with a geotherm of ~6 °C km^{-1}, lawsonite is always present at 1.1 to >4.0 GPa, and chlorite, glaucophane and talc can be stable at pressures of up to 2.3, 2.6 and 3.6 GPa respectively. Along such a *P–T* path, the density of subducted oceanic crust is always lower than that of the surrounding mantle at depths shallower than 110–120 km (< 3.3–3.6 GPa). However, along a warm subduction *P–T* path with a geotherm of ~10 °C km^{-1}, the *P–T* path is outside the stability field of lawsonite, and the hydrous minerals of chlorite, epidote and amphibole break down completely into dry dense minerals at relatively lower pressures of 1.5, 1.85 and 1.9 GPa respectively. Along such a warm subduction *P–T* path, the subducted oceanic crust becomes denser than the surrounding mantle at depths >60 km (>1.8 GPa). Oceanic eclogites with high H_2O content, oxygen fugacity, bulk-rock X_{Mg} [= MgO/(MgO + FeO)], X_{Al} [= Al_2O_3/(Al_2O_3 + MgO + FeO)] and low X_{Ca} [= CaO/(CaO + MgO + FeO + Na_2O)] are likely suitable for exhumation, which is consistent with the bulk-rock compositions of the natural oceanic eclogites on the Earth's surface. On the basis of natural observations and our calculations, it is suggested that beyond depths around 110–120 km oceanic eclogites are not light enough and/or there are no blueschists to compensate the negative buoyancy of the oceanic crust, therefore explaining the lack of oceanic eclogites returned from ultradeep mantle (>120 km) to the Earth's surface. The exhumed light–cold–hydrous oceanic eclogites may have decoupled from the top part of the sinking slab at shallow depths in the forearc region and are exhumed inside the serpentinized subduction channel, whereas the dense–hot–dry eclogites may be retained in the sinking slab and recycled into deeper mantle.

Key words: density; exhumation; hydrous minerals; subducted oceanic crust; thermodynamic modelling.

INTRODUCTION

Oceanic crust is composed primarily of MORB, and it is transformed into blueschist and high-pressure (HP) or ultrahigh-pressure (UHP) eclogite when it is subducted into mantle depths. Abundant experimental studies on MORB at HP and UHP conditions have shown that oceanic eclogites are denser than the surrounding mantle (e.g. Aoki & Takahashi, 2004; Litasov & Ohtani, 2005); therefore, oceanic eclogites are generally considered difficult to exhume to the surface when driven by buoyancy forces. Oceanic crust is commonly observed to be recycled into the transition zone (Zhao *et al.*, 2007; Zhao, 2008), the lower mantle (Fukao *et al.*, 2001) and even the core-mantle boundary (Hirose *et al.*, 1999; Karason & van der Hilst, 2000). However, some oceanic eclogites are exhumed to the surface in several oceanic subduction zones (e.g. Agard *et al.*, 2009; Wei *et al.*, 2009a; Brovarone *et al.*, 2011; Zhai *et al.*, 2011; Plunder *et al.*, 2012); some of them are even coesite-bearing UHP eclogites that were exhumed from mantle depths >90 km (Groppo *et al.*, 2009; Lü *et al.*, 2009; Angiboust *et al.*, 2012). The occurrence of natural HP and UHP oceanic eclogites indicates that at least parts of the subducted oceanic crust detached from the down-going slab and were exhumed back to the surface.

Several hypotheses have been proposed to explain the exhumation of these subducted oceanic eclogites. Shreve & Cloos (1986) and Platt (1986) suggested that part of the subducted oceanic crust and overlying sediments can be decoupled from the downgoing crust and dragged to crustal levels along the subduction channel by a low-density accretionary wedge. However, because the accretionary wedge is restricted to shallow depths (generally shallower than 40 km, Agard *et al.*, 2009), this model cannot explain the exhumation of deep subducted oceanic eclogites, especially UHP eclogites. An alternative hypothesis suggests that the subducted oceanic crust was dragged upward by the exhumed low-density continental rocks (e.g. Plunder *et al.*, 2012). However, in convergence plate boundaries involving both oceanic subduction and continental subduction, the subduction of oceanic crust is always prior to the subduction of continental crust, and the exhumation of oceanic eclogites is commonly prior to the HP–UHP rocks formed by continental subduction (Song *et al.*, 2006). A third hypothesis proposes that the exhumed oceanic eclogites were dragged upward by low-density serpentinite (Hermann *et al.*, 2000; Guillot *et al.*, 2001, 2009; Angiboust & Agard, 2010). Although this model is sufficient for the oceanic eclogites associated with serpentinite, such as those in Zermatt-Saas in the Western Alps (Angiboust & Agard, 2010), it cannot explain the exhumation of oceanic eclogites without serpentinite, such as those in Southwest Tianshan (Zhang *et al.*, 2008; Klemd *et al.*, 2011). Therefore, compared with the well-accepted buoyancy exhumation model for HP–UHP rocks formed by continental subduction (Davies & von Blanckenburg, 1995; Ernst, 2001), the exhumation mechanism associated with oceanic eclogites remains one of the least-known domains in the subduction factory (Gerya *et al.*, 2002; Gorczyk *et al.*, 2007; Krebs *et al.*, 2008; Blanco-Quintero *et al.*, 2010; Malatesta *et al.*, 2012).

All of the models above are based on the assumption that oceanic eclogites are denser than the surrounding mantle; therefore, their exhumation must be aided by low-density rocks. However, this raises the question of whether the natural oceanic eclogites are really denser than the upper mantle? We note that most of the exhumed oceanic eclogites at the surface are low-temperature hydrous eclogites formed at <3.2 GPa and <630 °C (e.g. Groppo *et al.*, 2009; Lü *et al.*, 2009; Wei *et al.*, 2009a; Angiboust & Agard, 2010; Brovarone *et al.*, 2011; Zhai et al., 2011; Angiboust *et al.*, 2012; Plunder *et al.*, 2012), and that no high-temperature oceanic eclogites have been reported. A typical feature of natural oceanic eclogites is that they are all enriched in low-density HP–UHP hydrous minerals, such as glaucophane, lawsonite, paragonite, phengite, talc and chloritoid. Their mineral assemblages and mineral proportions are quite different from those of the high-temperature eclogites produced in experiments. To achieve equilibrium quickly in the experimental systems and reduce the experimental durations, most experimental studies on the MORB were conducted at temperatures higher than 900 °C (e.g. Aoki & Takahashi, 2004; Litasov & Ohtani, 2005), and the high-temperature eclogites produced were relatively dry. The density data calibrated from such high-temperature dry eclogites obviously cannot represent the natural low-temperature hydrous oceanic eclogites observed. Even though a few experiments have extended investigations of phase relations in the MORB system to temperatures as low as 550 °C (Poli, 1993; Schmidt & Poli, 1998; Forneris & Holloway, 2003), no experimental density data are available for low-temperature hydrous oceanic eclogites. Therefore, the density of low-temperature hydrous oceanic eclogites remains unclear.

In this study, we calculated pseudosections for MORB compositions to constrain phase relations, mineral assemblages and mineral proportions under various *P–T* conditions. Based on these data, the densities of both low-temperature and high-temperature MORB eclogites were calculated, as well as the density evolution of oceanic eclogites along both a cold and a hot *P–T* path. The effects of the bulk-rock composition on the density of oceanic eclogites are also investigated. These data are used to constrain possible exhumation mechanisms for subducted oceanic eclogites worldwide.

NATURAL OCEANIC ECLOGITES

The oceanic eclogites reported in typical oceanic subduction zones worldwide are summarized in Table 1 and Fig. 1. They can be subdivided into three groups based on peak mineral assemblages and *P–T* conditions as follows: (i) Coesite-bearing UHP oceanic eclogites are reported in Zermatt-Saas and Monviso in the Western Alps (Groppo *et al.*, 2009; Angiboust & Agard, 2010; Angiboust *et al.*, 2012) and in Southwest Tianshan in China (Lü *et al.*, 2008, 2009). These UHP oceanic eclogites commonly contain lawsonite or pseudomorphs after lawsonite. They have a typical peak mineral assemblage of garnet + omphacite + lawsonite + coesite + phengite + rutile ± glaucophane, and their peak metamorphic *P–T* conditions are restricted to 2.7–3.2 GPa and 470–610 °C (Table 1; Fig. 1). Their peak metamorphic *P–T* conditions correspond to the geothermal gradients of 5–7 °C km^{-1}, corresponding to typical cold subduction (Fig. 1); (ii) HP lawsonite eclogites, including lawsonite-bearing or lawsonite pseudomorph-bearing eclogites, have been found in several cold oceanic subduction zones (Tsujimori *et al.*, 2006a, b; Wei & Clarke, 2011). They have a typical mineral assemblage of garnet + omphacite + lawsonite + glaucophane + phengite + quartz + rutile/titanite. Their peak *P–T* conditions are in the range of 1.7–2.6 GPa and 400–620 °C, corresponding to the geothermal gradients of 5–8 °C km^{-1} (Table 1; Fig. 1); and (iii) HP epidote eclogites are the most common type of

Table 1. Comparison of available data on natural oceanic eclogites (see also Fig. 1).

Type	No.	Locality	Estimated peak conditions (GPa/°C)	Mineral assemblage	X_{Mg}	X_{Al}	X_{Ca}	References
UHP eclogite	1	Zermatt-Saas, W. Alps	3.0–3.2/590–605	g + o + law* + coe + ru ± gl	0.46–0.74	0.29–0.46	0.17–0.46	Groppo *et al.* (2009); Angiboust & Agard (2010)
	2	Southwest Tianshan	2.7/470–510	g + o + law* + coe ± gl	0.41–0.76	0.27–0.42	0.15–0.36	Gao *et al.* (2007); Lü *et al.* (2009)
	3	Monviso, W. Alps	2.6–2.8/550	g + o + law* + q/coe + ru ± ctd	0.37–0.84	0.26–0.39	0.21–0.40	Groppo & Castelli (2010); Spandler *et al.* (2011); Angiboust *et al.* (2012)
HP law-eclogite	4	Schistes Lustres, Corsica	2.3/520	g + o + law + phe + q + tn	0.52–0.53	0.45–0.50	0.42–0.53	Brovarone *et al.* (2011); Plunder *et al.* (2012)
	5	Ward Creek, Franciscan Complex	1.8–2.2/420–460	g + o + law + gl + ep + chl + ru + q				Shibakusa & Maekawa (1997); Tsujimori *et al.* (2006b)
	6	Port Macquarie, Australia	2.0–2.4/524	g + o + law + phe + q + tn				Och *et al.* (2003)
	7	Guatemalan, Caribbean	2.5/520	g + o + law + gl + phe + q + ru ± chl				Tsujimori *et al.* (2006a); Endo *et al.* (2012)
	8	Pinchi Lake, British Columbia	2.4/505	g + o + law + gl + ta + phe + q + ru	0.57–0.67	0.32–0.37	0.29-0.32	Ghent *et al.* (2009)
	9	Sivrihisar Massif, Turkey	2.6/500	g + o + law + gl + phe + qu + q	0.51–0.63	0.32-0.39	0.41–0.43	Davis & Whitney (2006)
	10	Central Pontides, Turkey	1.7/400–430	g + o + law + phe + ru + q	0.60	0.27	0.29	Altherr *et al.* (2004); Okay *et al.* (2006)
	11	North Qilian	2.3–2.6/570–590	g + o + law* + gl + phe + q + ru	0.52–0.66	0.29–0.37	0.29–0.38	Song *et al.* (2006); Wei *et al.* (2009a); Cao *et al.* (2011)
	12	Samana, Dominica Republic	1.6/360	g + o + law + gl + pa + phe + q				Zack *et al.* (2004)
	13	Pam Peninsula, New Caledonia	2.1–2.4/470–580	g + o + law* + hb + phe + q + ru	0.38–0.61	0.27–0.33	0.27–0.29	Clarke *et al.* (1997); Marmo *et al.* (2002); Fitzherbert *et al.* (2003)
	14	Sulawesi, Indonesia	2.2–2.4/580–620	g + o + law* + gl + phe + ru + q				Miyazaki *et al.* (1996); Parkinson *et al.* (1998)
HP ep-eclogite	15	Sivrihisar Massif, Turkey	1.8/600	g + o + ep + amp + phe + ru + q	0.42–0.46	0.30–0.40	0.33–0.37	Davis & Whitney (2006)
	16	Franciscan, Tiburon	2.2–2.5/550–620	g + o + ep + amp + phe + ru + q ± pa	0.64	0.4	0.34	Saha *et al.* (2005); Tsujimori *et al.* (2006c)
	17	Voltri, W. Alps	2.0/550	g + o + pa + ta + ep + q + ru ± tn				Federico *et al.* (2004); Vignaroli *et al.* (2005)
	18	Omi serpentinite melange, SW Japan	1.8/550–600	g + o + gl + ep + q + ru + phe				Tsujimori & Matsumoto (2006)
	19	Southwest Mongolia	2.0–2.25/590–610	g + o + amp + ep + phe + q + ru				Štípská *et al.* (2010)
	20	Sanbagawa	2.0–2.2/590–600	g + o + amp + ep + q + ru + phe + hem	0.51-0.60	0.31-0.39	0.24-0.28	Wallis *et al.* (2000); Kabir & Takasu (2010)
	21	Adean Raspas Complex, Ecuador	1.8–2.0/550–600	g + o + amp + ep + phe + ru + tn + q	0.45-0.57	0.25-0.39	0.28-0.36	Bosch *et al.* (2002); John *et al.* (2010)
	22	Escambray Massif, Central Cuba	1.6–2.1/600	g + o + ep + amp + phe + ru + q	0.46-0.61	0.28-0.48	0.32-0.35	Schneider *et al.* (2004); Stanek *et al.* (2006)
	23	Sanandaj-Sirjan zone, Zagros	2.1–2.4/590–630	g + o + amp + ep + phe + ru + q				Davoudian *et al.* (2008)
	24	Sistan Suture Zone, Iran	1.9–2.3/600	g + o + amp + ep + phe + pa + ru + q				Fotoohi Rad *et al.* (2005)
	25	N. Serpentinite Melange, N. Cuba	1.5–2.0/600	g + o + amp + ep + ru + q				García-Casco *et al.* (2002, 2006)

Abbreviations: g: garnet; o: omphacite; law: lawsonite; law*: lawsonite pseudomorph; gl: glaucophane; ep: epidote; chl: chlorite; ctd: chloritoid; phe: phengite; ta: talc; pa: paragonite; hb: hornblende; amp: amphibole; tn: titanite; ru: rutile; hem: hematite; coe: coesite; q: quartz.

oceanic eclogites. They usually have a peak mineral assemblage of garnet + omphacite + epidote + amphibole (glaucophane, barroisite, actinolite or hornblende) + phengite + quartz + rutile/titanite. They have slightly lower peak pressures and higher peak temperatures (1.5–2.3 GPa, 540–630 °C) relative to the lawsonite eclogites (Table 1; Fig. 1). Their peak metamorphic *P–T* conditions correspond to the geothermal gradients of 7–12 °C km^{-1} (Fig. 1). They represent the products of warm subduction (Tsujimori & Matsumoto, 2006; Kabir & Takasu, 2010) or isothermal decompression of HP lawsonite eclogites (Davis & Whitney, 2006; Wei & Clarke, 2011).

Compared with HP and UHP eclogites in continental subduction–collision zones, oceanic eclogites have three distinctive characteristics. (i) Only rare oceanic eclogites record UHP metamorphism, and their peak pressures are <3.2 GPa (Fig. 1) (Zhang *et al.*, 2008; Agard *et al.*, 2009). Most of the associated serpentinized mantle peridotites are spinel-facies peridotite (<80 km, e.g. Guillot *et al.*, 2001). These data suggest that both the oceanic eclogites and the associated mantle peridotites were exhumed from maximum depths of ~100 km; (ii) almost all of the natural oceanic eclogites are low-temperature eclogites (<630 °C). This result suggests that the high-temperature eclogites in the

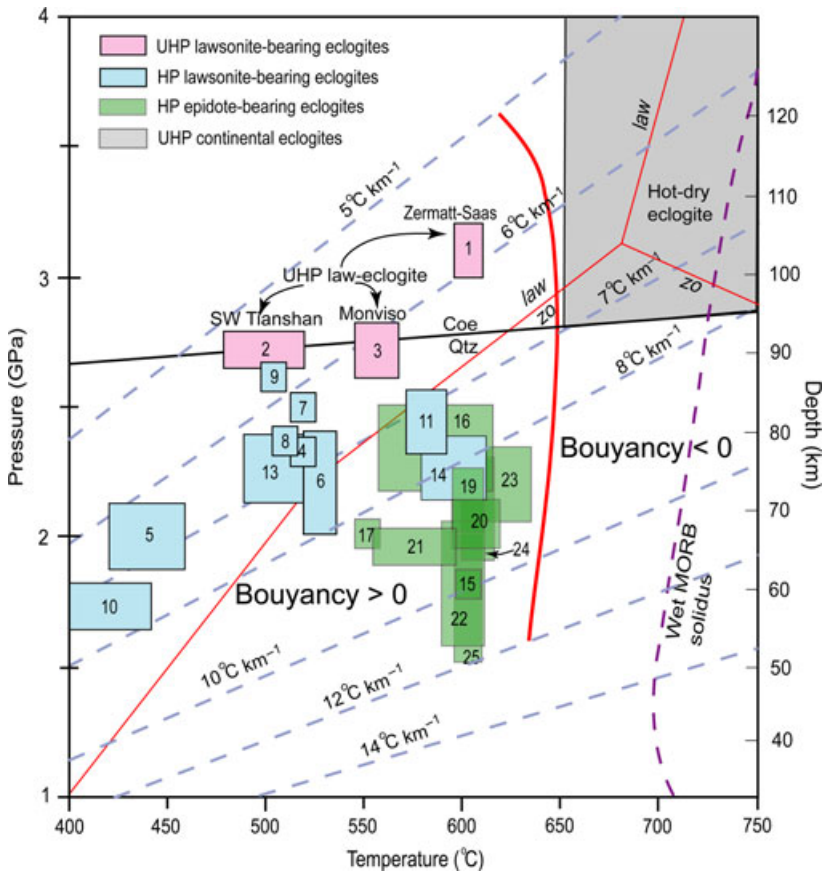

Fig. 1. Plots of the peak metamorphic *P–T* conditions of the reported natural oceanic eclogites (the numbers are the same as in Table 1). For comparison, the estimated *P–T* region of UHP continental eclogites is also shown. The lawsonite and zoisite stability curves and the wet MORB solidus were taken from Schmidt & Poli (1998). The transition of quartz and coesite was calculated using THERMOCALC. The red solid line is depth limit curve for the exhumation of oceanic eclogites calculated on the basis of various geothermal gradients. The left side of the curve represents the *P–T* region that is suitable for buoyancy-driven exhumation. Note that all of the estimated *P–T* conditions associated with the worldwide natural oceanic eclogites are located within the left side of the curve.

subducted oceanic crust may have recycled into the deep mantle and cannot be exhumed back to the surface; and (iii) the natural oceanic eclogites are enriched in light hydrous minerals, such as glaucophane (density: 3.14 g cm^{-3}), phengite (2.80 g cm^{-3}), lawsonite (3.13 g cm^{-3}), chlorite (2.58 g cm^{-3}) and talc (2.73 g cm^{-3}) (Hacker *et al.*, 2003). In some cases, the total content of light hydrous minerals can be up to 70 vol% (e.g. Ghent *et al.*, 2009). Compared with the continental HP–UHP eclogites, the contents of dense garnet (4.06 g cm^{-3}) and omphacite (3.36 g cm^{-3}) are much lower. Kyanite (3.58 g cm^{-3}), a common dense mineral in high-temperature eclogites, is extremely rare in natural oceanic eclogites (Table 1). Given that the densities of light hydrous minerals are lower than those of normal lithospheric mantle (~3.37 g cm^{-3}, Dziewonski & Anderson, 1981), their enrichment may play an important role in the exhumation of oceanic eclogites.

METHODOLOGY

Calculation method

Quantitative pseudosections calculated using an internally consistent thermodynamic data set (Holland & Powell, 1998) and the software THERMOCALC (Powell *et al.*, 1998) have proven to be a powerful approach to predict phase relations for a specific bulk-rock composition. They can be used to calculate mineral assemblages, mineral compositions and mineral proportions in a given rock under various *P–T* conditions when the volume of rock under consideration reaches chemical equilibrium (Powell & Holland, 2008). On the other hand, the densities of any rock-forming mineral under any *P–T* conditions can be calculated on the basis of its thermoelastic parameters (e.g. Hacker *et al.*, 2003). However, the method of Hacker *et al.* (2003) treated each mineral assemblage as containing constant mineral compositions and proportions, with the density only varying as a function of *P–T* within a given assemblage. The only difficulty in applying the method of Hacker *et al.* (2003) is to model the mineral assemblages, compositions and proportions; however, such problem can be solved by phase diagram calculations. Therefore, by combining phase diagram calculations and the method of Hacker *et al.* (2003), the density of a whole rock can be calculated under various *P–T* conditions. In this study, we take the expression for density developed in Appendix A in Hacker *et al.* (2003), the association parameter values from Table 1 in Hacker *et al.* (2003) and the resulting expressions are applied to the mineral compositions and proportions that were calculated using THERMOCALC. This method fully considers the effects of pressure,

temperature, mineral compositions and proportions on the whole-rock density. A similar approach has been successfully applied in the calculation of densities of HP–UHP rocks in the subduction slab (e.g. Angiboust & Agard, 2010; van Keken *et al*., 2011); however, the phase equilibria modelling in the previous studies was performed using Perple_X program (Connolly, 1990).

The pseudosections were calculated using THERMOCALC 3.33 (Powell *et al*., 1998; and upgrades) and the internally consistent thermodynamic data set (file tc-ds55.txt) of Holland & Powell (1998). The pseudosections constructed involves actinolite (act), biotite (bi), chlorite (chl), stishovite (stv), coesite (coe), quartz (q), diopside (di), epidote (ep), garnet (g), glaucophane (gl), hornblende (hb), ilmenite (ilm), jadeite (jd), kyanite (ky), lawsonite (law), phengitic muscovite (mu), omphacite (omp), orthopyroxene (opx), plagioclase (pl), talc (ta) and liquid (liq). The activity-composition models of solid minerals used in this study are those presented for amphibole (Diener *et al*., 2007), chlorite (Holland *et al*., 1998), clinopyroxene (Green *et al*., 2007), epidote and talc (Holland & Powell, 1998), garnet (White *et al*., 2007), paragonite and phengitic muscovite (Coggon & Holland, 2002), and plagioclase (Holland & Powell, 2003). Lawsonite, kyanite, rutile and stishovite/coesite/quartz are treated as pure end-member phases.

Uncertainties in modelling

The model and density calculations in this article are affected by: (i) uncertainties in the predicted mineral assemblages, mineral modes, and mineral end-member activities in the pseudosection calculations; and (ii) uncertainties in the density calculations for each end-member. Hacker *et al*. (2003) reproduced the rock densities measured in laboratories to within 2%, based on their density calculation method. However, it is very hard to estimate the uncertainties associated with the activity models in the pseudosection calculations quantitatively, as this information cannot easily be extracted from THERMOCALC (Powell & Holland, 2008). Numerous previous studies (e.g. Rebay *et al*., 2010; Wei & Clarke, 2011) indicate that the activity-composition models in pseudosection calculations work adequately below 3 GPa. The validity of activity-composition models at higher pressures (>3 GPa) should be carefully checked. The best way to estimate the uncertainties in the pseudosection and density calculations altogether is to reproduce the phase relations and rock densities constrained by high-pressure experiments on hot, dry eclogites. All these experiments were conducted at high-temperatures above the solidus. Unfortunately, an activity-composition model for melt in MORB compositions or at such high pressures is not available. Therefore, it is only possible to model experimental results on pelitic–felsic rocks (White *et al*., 2011).

Wu *et al*. (2009) conducted a series of experiments in a P–T range of 3.5–24 GPa and 750–1800 °C on a natural UHP paragneiss from Shuanghe in the Dabie UHP terrane to constrain the phase relations and density evolution of subducted upper continental crust. They calculated density profiles along a cold and a hot subduction geotherm, respectively, based on the phase relations constrained by their experiments (Fig. 2b). In this article, we construct a P–T pseudosection (Fig. 2a) in the available range of 1–7 GPa and 400–1000 °C in the NCKFMASHTO system using the composition of the starting material of Wu *et al*. (2009). The phase relations at higher pressure conditions were not calculated, due to lack of suitable activity-composition models for UHP phases such as K-hollandite and perovskite. Our calculated mineral assemblages are very consistent with those produced by the experiments of Wu *et al*. (2009) in the given P–T range (Fig. 2a). Only minor excess kyanite (3.8 mol.%) and muscovite (2.8 mol.%) occur in the modelled P–T pseudosection at 3.5 GPa and 1000 °C, probably due to uncertainties of activity-composition models of minerals. The consistency in mineral assemblages between our calculated results and the experimental results of Wu *et al*. (2009) suggests THERMOCALC modelling can also work well at high pressures (>3 GPa). Based on the calculated mineral assemblages, mineral proportions and mineral compositions, the densities of the whole rock were calculated in the given P–T range using the method proposed by Hacker *et al*. (2003). For comparison, the calculated density profiles (Fig. 2b) were plotted along the cold and hot subduction geotherms employed by Wu *et al*. (2009). Figure 2b shows that our calculated densities also match well those constrained by Wu *et al*. (2009). These applications show that the thermodynamic modelling and density calculation methods applied in this article are valid and it is reasonable to apply these calculation methods to reveal detailed phase relations and rock densities of the subduction oceanic crust.

In addition, the model and density calculations in this article may also differ slightly from the natural oceanic eclogites, as compositional zoning in minerals such as garnet, omphacite and glaucophane are common in low-temperature eclogites and such features are not considered in the modelling. In this article, several comparisons (including pressure, temperature, exhumation depth and bulk composition) between the models and observations are made to check the validity of modelling.

PHASE RELATIONS AND DENSITY EVOLUTION OF SUBDUCTED MORB

Bulk-rock composition of MORB

The average composition of 103 unaltered MORB samples from eight mid-ocean ridges (Cottrell &

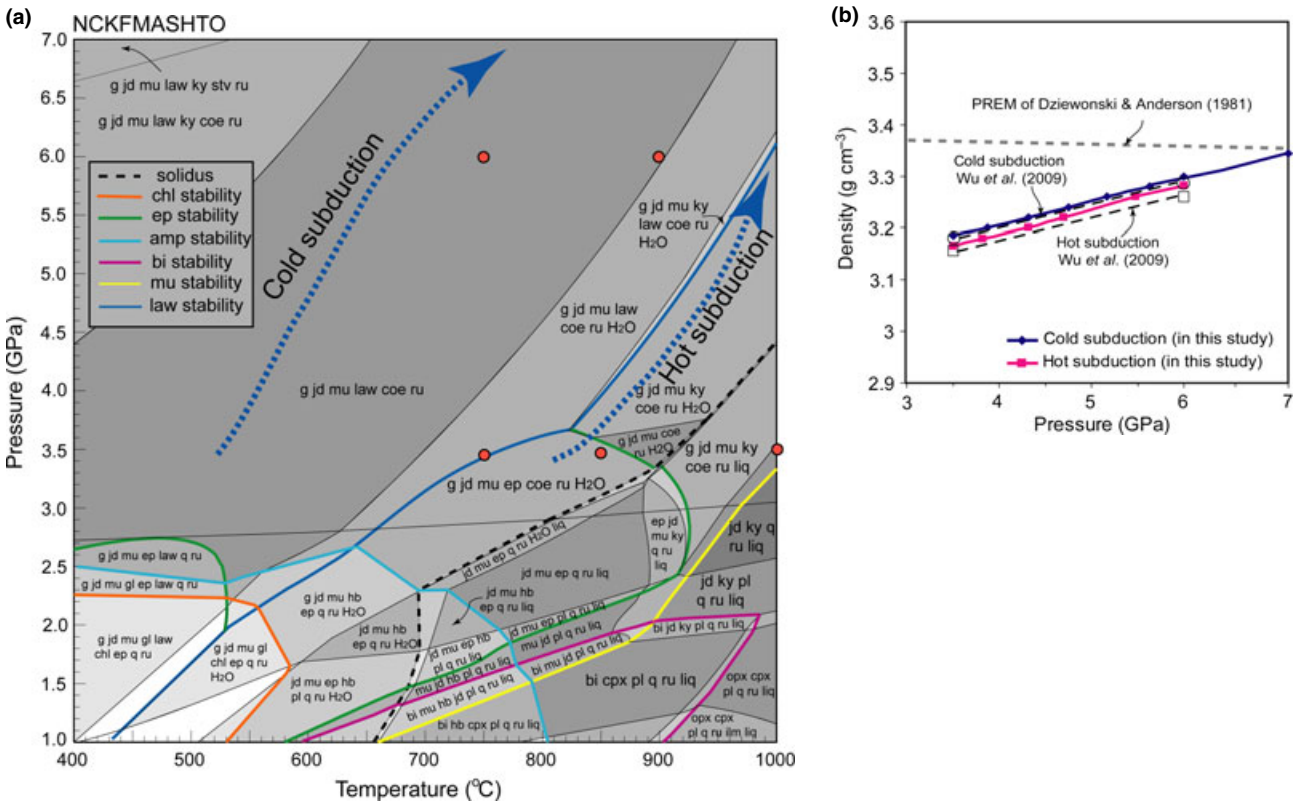

Fig. 2. (a) *P–T* pseudosection in the system NCKFMASHTO for the paragneiss from Shuanghe in the Dabie UHP terrane used by Wu *et al.* (2009). The stabilities of hydrous minerals are also shown. The cold and hot *P–T* paths are after Wu *et al.* (2009). The five red circles plotted in the pseudosection represent the *P–T* conditions conducted in experiments by Wu *et al.* (2009). (b) Comparison of the density profiles calculated in this study and those modelled by Wu *et al.* (2009). The density profile of the surrounding mantle is derived from PREM (Dziewonski & Anderson, 1981). For mineral abbreviations see the main text.

Kelley, 2011) was used to calculate pseudosections in this study. This composition was comprised of the following (in wt%): SiO_2 = 50.51, TiO_2 = 1.39, Al_2O_3 = 15.70, FeO = 9.46, MnO = 0.18, MgO = 7.94, CaO = 11.58, Na_2O = 2.70, K_2O = 0.16, and P_2O_5 = 0.16. The composition was normalized to the Na_2O–CaO–K_2O–FeO–MgO–Al_2O_3–SiO_2–H_2O–TiO_2–Fe_2O_3 (NCKFMASHTO) system, and the minor components of MnO and P_2O_5 were neglected because they are mainly contained in garnet and apatite and incorporated only in very small amounts in the main silicate minerals. The fluid was assumed to be pure H_2O. As the natural oceanic eclogites currently have higher Fe^{3+} than the unaltered MORB (X_{Fe3+} = $Fe^{3+}/[Fe^{2+} + Fe^{3+}]$ = 0.12–0.16, Bezos & Humler, 2005; Cottrell & Kelley, 2011), we chose 32% conversion of all Fe as FeO to Fe_2O_3 (X_{Fe3+} = 0.32), similar X_{Fe3+} value was also used by Rebay *et al.* (2010). In the later section, the effect of Fe^{3+} on phase relations and densities is discussed. As fractional crystallization can significantly affect the MgO, FeO, CaO and Al_2O_3 contents of oceanic crust, the effects of various MgO, FeO, CaO and Al_2O_3 contents on phase relations and densities should also be evaluated for the chosen rock composition.

Phase relations for subducted MORB

A H_2O-saturated *P–T* pseudosection was calculated using the given average MORB composition in the *P–T* range of 1–4 GPa and 400–800 °C (Fig. 3). Muscovite and rutile are stable across this *P–T* range because K_2O and TiO_2 are primarily concentrated in these two minerals respectively. Ilmenite and titanite, which are commonly formed during the retrograde metamorphism of oceanic eclogites, may be stable at pressures of <1.5 GPa; however, these two minerals were not predicted in this pseudosection.

The pseudosection (Fig. 3) shows that each hydrous mineral has a specific *P–T* stability field. Chlorite is stable under low-*T* conditions (<590 °C), epidote is stable under low-*P* conditions (<2.4 GPa) and talc appears under high-*P* (>2.0 GPa) and low-*T* (<650 °C) conditions. The maximum pressure of glaucophane stability decreases with increasing temperature (Fig. 3). Glaucophane is predicted to be stable below 630 °C; this calculated result is close to the experimental results for the MORB system (e.g. Schmidt & Poli, 1998). Lawsonite is stable over a large *P–T* range, and lawsonite + epidote assemblages are only present in a narrow transitional zone,

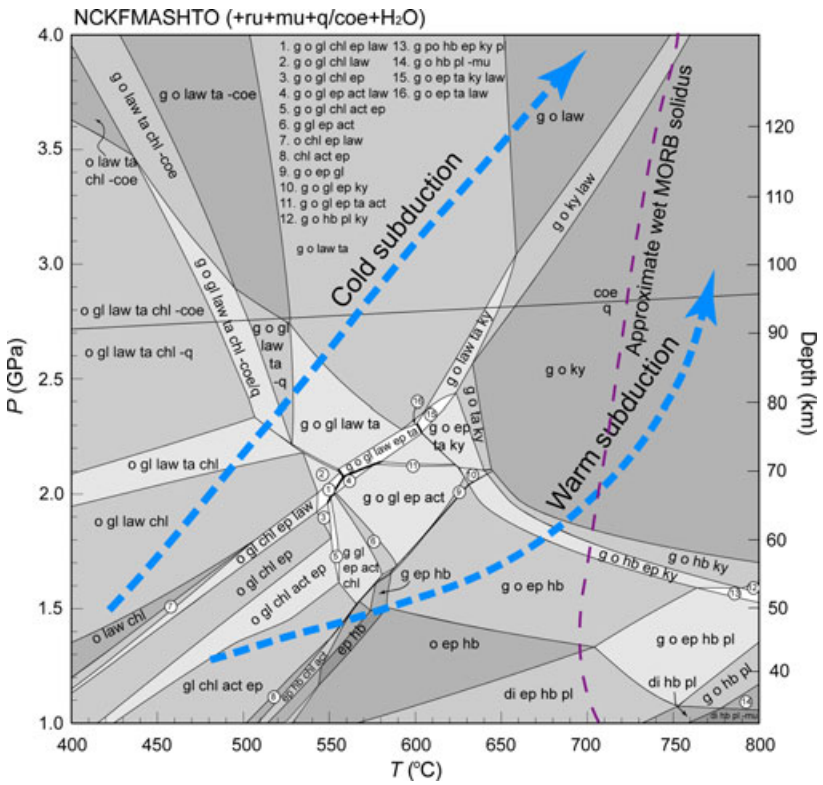

Fig. 3. The calculated *P–T* pseudosection in the NCKFMASHTO system (+ ru + mu + q/coe + H_2O) based on the average MORB composition (Cottrell & Kelley, 2011), recalculated on the basis of normalized mol.% to SiO_2 = 52.10, Al_2O_3 = 9.55, CaO = 12.79, MgO = 12.21, FeO = 8.16, K_2O = 0.11, Na_2O = 2.70, TiO_2 = 1.08, and O = 1.31. This base composition is used for all of following pseudosections. Rutile, muscovite, quartz/coesite and H_2O are present in all fields except in those marked as (-q) and (-coe), which signify the absence of quartz and coesite respectively. The wet MORB solidus was taken from Schmidt & Poli (1998). The cold and warm *P–T* paths discussed in the text are also shown. For mineral abbreviations see the main text.

which is controlled by the lawsonite breakdown reactions. Kyanite is a typical high-pressure, high-temperature phase; it is stable at pressures of >1.5 GPa and at temperatures higher than 600 °C. The calculated stability of epidote is different from experimentally determined results (Fig. 1), probably due to the different bulk-rock compositions used in pseudosection calculation and experimental starting material or the large uncertainty in *P–T* estimation using different approaches.

It remains known that different subduction slabs have different thermal structures (Peacock & Wang, 1999; Kirby, 2000). To investigate the metamorphic and density variations of cold and warm subducted oceanic crusts, cold (~6 °C km^{-1}) and warm (~10 °C km^{-1}) *P–T* paths were considered in this study (Fig. 3). The *P–T* pseudosection shows that the phase assemblages developed by the chosen bulk composition along the cold *P–T* path are quite different from those along the warm *P–T* path.

Along the cold *P–T* path, the subducted MORB is transformed from the blueschist facies assemblage of o + gl + law + chl ± ta to the eclogite facies assemblage of g + o + law ± ta ± chl ± gl (+ mu + q/coe + H_2O). The mineral proportions and H_2O content along the cold *P–T* path are shown in Fig. 4a. The H_2O content (wt%) shown in Fig. 4 is the H_2O bound in the minerals, it refers to that just required to saturate the corresponding mineral assemblages. Changes in mineral proportions and bound H_2O content suggest that prograde dehydration reactions occur during the subduction of cold oceanic crust. With increasing pressure, chlorite, glaucophane and talc are completely consumed at pressures of 2.3, 2.6 and 3.6 GPa respectively; lawsonite will completely break down under much higher pressures. These dehydration pressures correspond to those at the depth (80–150 km) of the subduction slab just under the island arc (Manning, 2004).

Along the warm *P–T* path (~10 °C km^{-1}), the subducted MORB is transformed from an amphibolite facies assemblage of amp + chl + ep ± o to an eclogite facies assemblage of g + o ± ep ± amp ± ky (+ mu + q/coe + H_2O). The mineral proportions and bound H_2O content along the warm *P–T* path are given in Fig. 4b, which shows that the bound H_2O content in the warm subducted MORB is significantly lower than that in the cold subducted MORB. Figure 4b indicates that, along the warm *P–T* path, the hydrous minerals chlorite, epidote and amphibole also break down over a wide *P–T* range. However, in contrast to the case of cold subduction, the hydrous minerals chlorite, epidote and amphibole are consumed along the warm path at relatively lower pressures of 1.5, 1.88 and 1.9 GPa respectively. Warm oceanic eclogites become almost dry at pressures of >1.9 GPa (>60 km), and only a small amount of H_2O (~0.06 wt%) is contained in phengite, indicating that the warm subducted oceanic crust cannot transport a significant amount of H_2O to the deep mantle.

Density evolution of subducted MORB in the shallow mantle

Figure 4c shows the calculated density profiles along the cold and warm *P–T* paths illustrated in Fig. 3. With the increase in *P–T*, the density of the cold subducted oceanic crust increases slowly from 3.12 g cm^{-3} at 1.5 GPa to 3.46 g cm^{-3} at 4 GPa. However, the density of the warm subducted oceanic crust increases quickly from 3.21 g cm^{-3} at 1.2 GPa to 3.45 g cm^{-3} at 1.9 GPa and then increases slowly to 3.49 g cm^{-3} at 3 GPa. Considering the mineral assemblage changes (Fig. 4a,b), the density evolution of subducted oceanic crust is mainly controlled by the dehydration reactions of the light hydrous minerals. When the dehydration reactions occur, the density increases sharply (Fig. 4c). For example, along the cold subduction *P–T* path, chlorite, glaucophane and talc are stable under HP and UHP conditions. Their presence results in the relatively low density of the subducted cold and hydrous oceanic crust under relatively high pressure conditions (Fig. 4c), and the breakdown of these minerals produces denser minerals (e.g. garnet and omphacite), releases low-density hydrous fluid and thus results in the sharp density increase in the cold subducted oceanic crust. However, even though chlorite and glaucophane are completely consumed at pressures of ~2.5 GPa, the cold subducted oceanic crust still has high proportions of talc and lawsonite (Fig. 4a), and the density of the cold subducted oceanic crust is still <3.30 g cm^{-3} at pressures as high as 3.0 GPa (Fig. 4c). In contrast, along the warm subduction *P–T* path, lawsonite is not stable, and all chlorite, epidote and amphibole are consumed at pressures of <1.9 GPa (Fig. 4b); their breakdown results in a rapid increase in the density of the warm subducted oceanic crust at relatively shallow depths (<60 km) (Fig. 4c). After the breakdown of amphibole at pressures of <1.9 GPa, the warm subducted oceanic crust becomes relatively dry. It should be noted that once the *P–T* path crosses the wet solidus of MORB (for example, 2.0 GPa and 700 °C; Fig. 3), the density of the warm subducted oceanic crust should be higher than that shown in Fig. 4c.

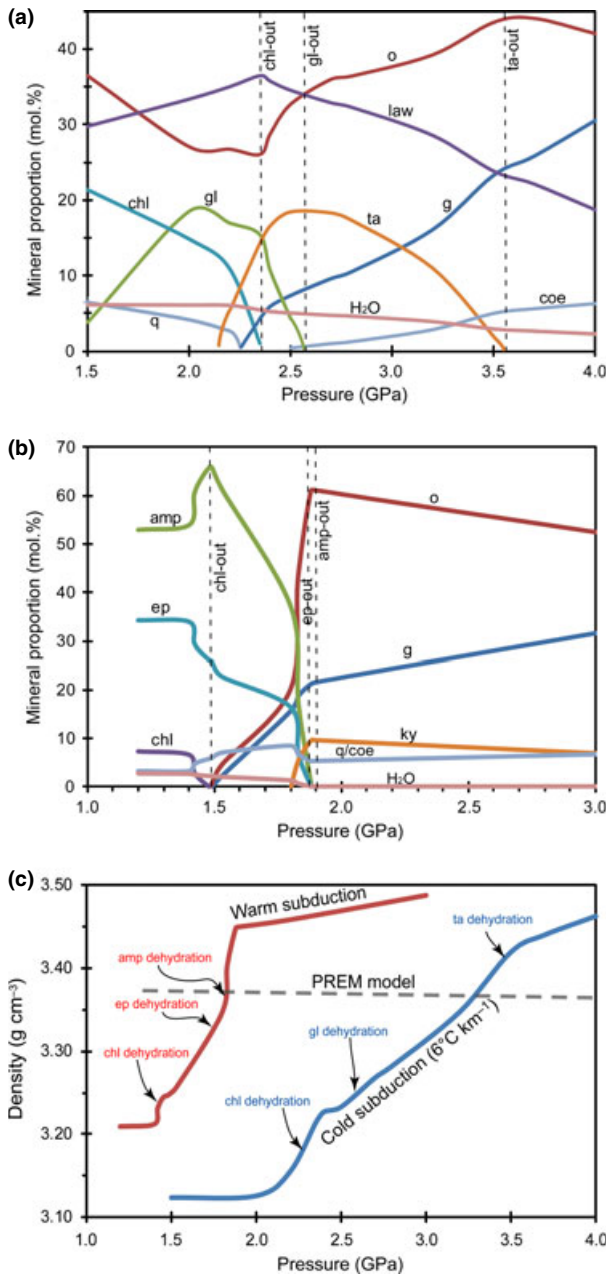

Fig. 4. Calculated modal proportions of the major minerals and H_2O contained in solid phases along the geotherms of cold (6 °C km^{-1}, a) and warm (10 °C km^{-1}, b) subductions. (c) The calculated density profiles of the subducted oceanic crust along the cold and warm subductions shown in Fig. 3. The density profile of mantle derived from PREM (Dziewonski & Anderson, 1981) is also shown.

EFFECTS OF BULK COMPOSITION ON THE DENSITY OF OCEANIC ECLOGITES

Many studies have revealed that phase relations are also significantly influenced by the chosen bulk-rock composition, H_2O content and oxidation state (Powell *et al.*, 2005; Clarke *et al.*, 2006; Angiboust & Agard, 2010; Rebay *et al.*, 2010; Wei & Clarke, 2011), thus also influence the density of the subducted oceanic crust. Abundant geochemical studies indicate that the oceanic eclogites have typically compositional features of mid-ocean ridge basalt (MORB) or ocean-island basalt (OIB), with variable X_{Mg} (molecular ratio of MgO/[MgO + FeO]) from 0.3 to 0.8 (Table 1) (e.g. Wallis *et al.*, 2000; Bosch *et al.*, 2002; Fitzherbert *et al.*, 2003; Song *et al.*, 2006; Gao *et al.*, 2007). Further, the changes of oxidation–reduction conditions and fluid activity during the subduction process commonly result in higher Fe^{3+} in oceanic eclogites than that in unaltered MORB (Rebay *et al.*, 2010). Therefore, the effects of H_2O content, bulk-rock

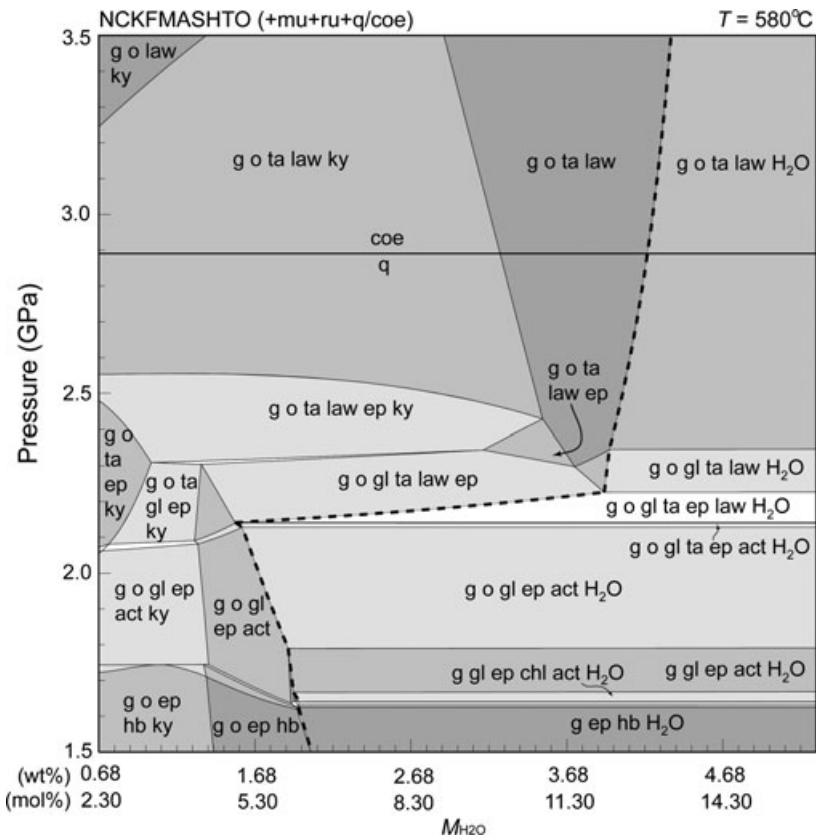

Fig. 5. P–M_{H2O} (wt%) pseudosection in the NCKFMASHTO system (+ mu + ru + q/coe) for the MORB composition in Fig. 3, calculated at 580 °C. The thick dash line shows the H_2O-saturation line.

composition and oxidation state on the density of oceanic eclogites should be carefully considered.

H_2O content

To investigate the effect of H_2O content on the phase relations under eclogite facies conditions, we calculated a P–M_{H_2O} pseudosection at 580 °C (Fig. 5). The weight percentage of H_2O was adjusted, but the bulk-rock composition remained unchanged. The P–M_{H_2O} pseudosection reveals that the H_2O saturation varies at different pressures: (i) M_{H_2O} = 1.60–2.05 wt% at <2.1 GPa; (ii) M_{H_2O} = 1.60–3.90 wt% at 2.1–2.4 GPa; and (iii) M_{H_2O} = 3.90–4.27 wt% at >2.4 GPa. The variation in the H_2O saturation of the entire rock is clearly controlled by the stability of the hydrous minerals, with for example, the formation of lawsonite at >2.1 GPa consumes high amounts of H_2O; therefore, the whole-rock saturation H_2O content increases from 1.60 wt% at 2.1 GPa to 4.27 wt% at 3.5 GPa. Under H_2O-saturated conditions (fluid-present), the mineral assemblages are not affected by the H_2O content; however, under H_2O-undersaturated conditions (fluid-absent), the mineral assemblages change significantly with the H_2O content. Under H_2O-undersaturated conditions, the stabilities of amphibole (glaucophane) and talc are restricted at nearly constant pressures, but the stability of epidote is enlarged to higher pressures. Under H_2O-undersaturated conditions, kyanite is stable at almost all model pressures; however, it is absent under H_2O-saturated conditions (Fig. 5).

To investigate the effect of H_2O content on the density of the subducted oceanic crust, the changes in mineral proportions and rock densities were calculated with H_2O content at 2.0 GPa (Fig. 6a), 2.5 GPa (Fig. 6b) and 3.0 GPa (Fig. 6c); the modelling temperature remained at 580 °C, the modelling P–T conditions corresponded to the geothermal gradient of 6–8 °C km^{-1}, and the modelling mineral assemblages were HP epidote–eclogite facies (2.0 GPa, Fig. 6a), HP lawsonite-eclogite facies (2.5 GPa, Fig. 6b) and UHP lawsonite-eclogite facies (3.0 GPa, Fig. 6c) respectively. Although the peak temperature conditions of most HP lawsonite eclogites are slightly lower than 580 °C (Fig. 1), the lower temperatures would stabilize higher proportions of light hydrous minerals, resulting in lower rock densities. Therefore, most lawsonite eclogites summarized in Fig. 1 probably have slightly lower densities than those we constrained at 580 °C. Under H_2O-undersaturated conditions, the proportions of all hydrous minerals are positively correlated with H_2O content; in contrast, the proportions of the dense anhydrous minerals (garnet, kyanite and omphacite) decrease with increasing H_2O content. As a consequence, the density of subducted oceanic crust decreases gradually with the increase in H_2O content.

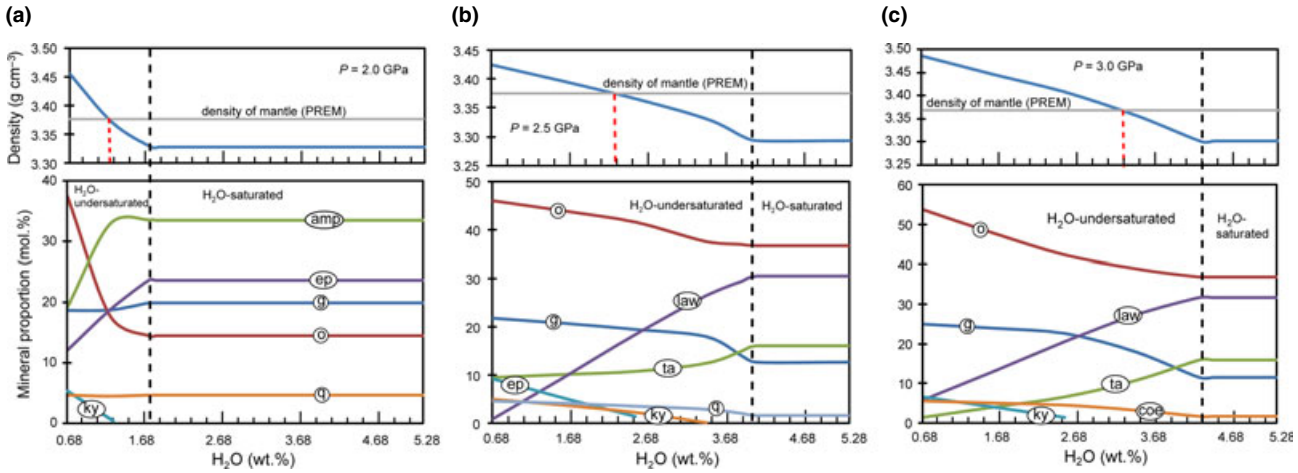

Fig. 6. Calculated mineral proportions and rock densities with varying H_2O content on the basis of Fig. 5 at 2.0 (a), 2.5 (b) and 3.0 (c) GPa. The density of the surrounding mantle is based on PREM (Dziewonski & Anderson, 1981). The black dashed lines represent the H_2O-saturated contents.

Bulk-rock X_{Mg}

To illustrate the effects of bulk-rock X_{Mg} on mineral assemblage under eclogite facies conditions, two pseudosections of P–X_{Mg} at 580 °C (Fig. 7a) and T–X_{Mg} at 2.5 GPa (Fig. 7b) were calculated. Mole proportions of MgO and FeO were adjusted with a fixed $Fe^{3+}/Fe_{total} = 0.32$, but mole proportions of other components remain unchanged. Figure 7 shows that increasing X_{Mg} reduces the stability fields of garnet to higher pressures and temperatures but expands the stability fields of chlorite, glaucophane and talc; increasing X_{Mg} slightly reduces the stability field of epidote to lower pressures (Fig. 7b). At 2.5 GPa and >570 °C, epidote is stable only at X_{Mg}<0.54 (Fig. 7b). The dense kyanite occurs only in rocks with X_{Mg}>0.16 at >610 °C (Fig. 7b). The stability of lawsonite is not significantly affected by X_{Mg}.

Figure 8a shows the variation of mineral proportions with varying X_{Mg} at 2.5 GPa and 580 °C. Increasing X_{Mg} decreases the proportions of garnet, epidote and quartz, but increases the proportions of the light hydrous minerals such as lawsonite, talc and chlorite. Figure 8b illustrates the variation of rock density with X_{Mg} at 2.0 GPa, 2.5 GPa, and 3.0 GPa, respectively. At any P–T conditions, the density of subducted oceanic crust decreases significantly with the increase of X_{Mg}. Figure 8b also reveals that the HP epidote blueschist/eclogite (2.0 GPa) is much denser than the HP (2.5 GPa) and UHP (3.0 GPa) lawsonite eclogites in Mg-rich system (X_{Mg}>0.5).

Bulk-rock X_{Al}

Bulk-rock X_{Al} [= $Al_2O_3/(Al_2O_3 + MgO + FeO)$ in mol.%] controls the stabilities and proportions of the Al-rich rock-forming minerals. Dense anhydrous garnet and kyanite are typical Al-rich minerals in eclogite; light hydrous lawsonite is also an Al-rich mineral in low-T eclogite. Therefore, it is worth investigating the effect of bulk-rock X_{Al} on mineral assemblage, mineral proportions and whole-rock density of the subducted oceanic crust. Two pseudosections, a P–X_{Al} at 580 °C (Fig. 9a) and a T–X_{Al} at 2.5 GPa (Fig. 9b), were calculated. Mole proportion of Al_2O_3 was adjusted with a fixed X_{Mg} (= 0.60) and Fe^{3+}/Fe_{total} (= 0.32), with the x-axis varying from Al_2O_3 = 6.00, MgO = 14.39, FeO = 9.62 and O = 1.54 (X_{Al} = 0.20) to Al_2O_3 = 15.01, MgO = 9.00, FeO = 6.01 and O = 0.96 (X_{Al} = 0.50); the mole proportions of other components remain unchanged. The P–X_{Al} pseudosection (Fig. 9a) indicates that increasing X_{Al} expands the stability of glaucophane to higher pressures up to 3.2 GPa at X_{Al} = 0.5, and restricts the stability of omphacite-bearing fields to higher pressures. Chlorite is restricted to high X_{Al}>0.32, and chloritoid is restricted to X_{Al}>0.39 (Fig. 9a). The T–X_{Al} pseudosection (Fig. 9b) shows that kyanite is restricted to temperatures higher than 600 °C, and the increase of X_{Al} slightly shifts the kyanite-bearing assemblages to lower temperatures. Epidote is restricted to high X_{Al} fields (>0.37) and at temperatures above 630 °C. The stabilities of lawsonite and talc are not significantly affected by X_{Al}.

Figure 10a shows the effect of X_{Al} on mineral proportions in the HP lawsonite eclogite at 2.5 GPa and 580 °C. Increasing X_{Al} decreases the proportions of garnet, omphacite and talc, which are compensated by the increase in lawsonite and glaucophane (Fig. 10a). As the increase of bulk-rock X_{Al} can significantly increase the proportions of both light lawsonite and dense kyanite and epidote, the X_{Al}–density relationships were calculated at five P–T conditions: (i) 2.0 GPa and 580 °C corresponding to HP epidote eclogite; (ii) 2.5 GPa and 580 °C corresponding to HP lawsonite eclogite; (iii) 3.0 GPa and 580 °C corresponding to UHP lawsonite eclogite; and (iv)

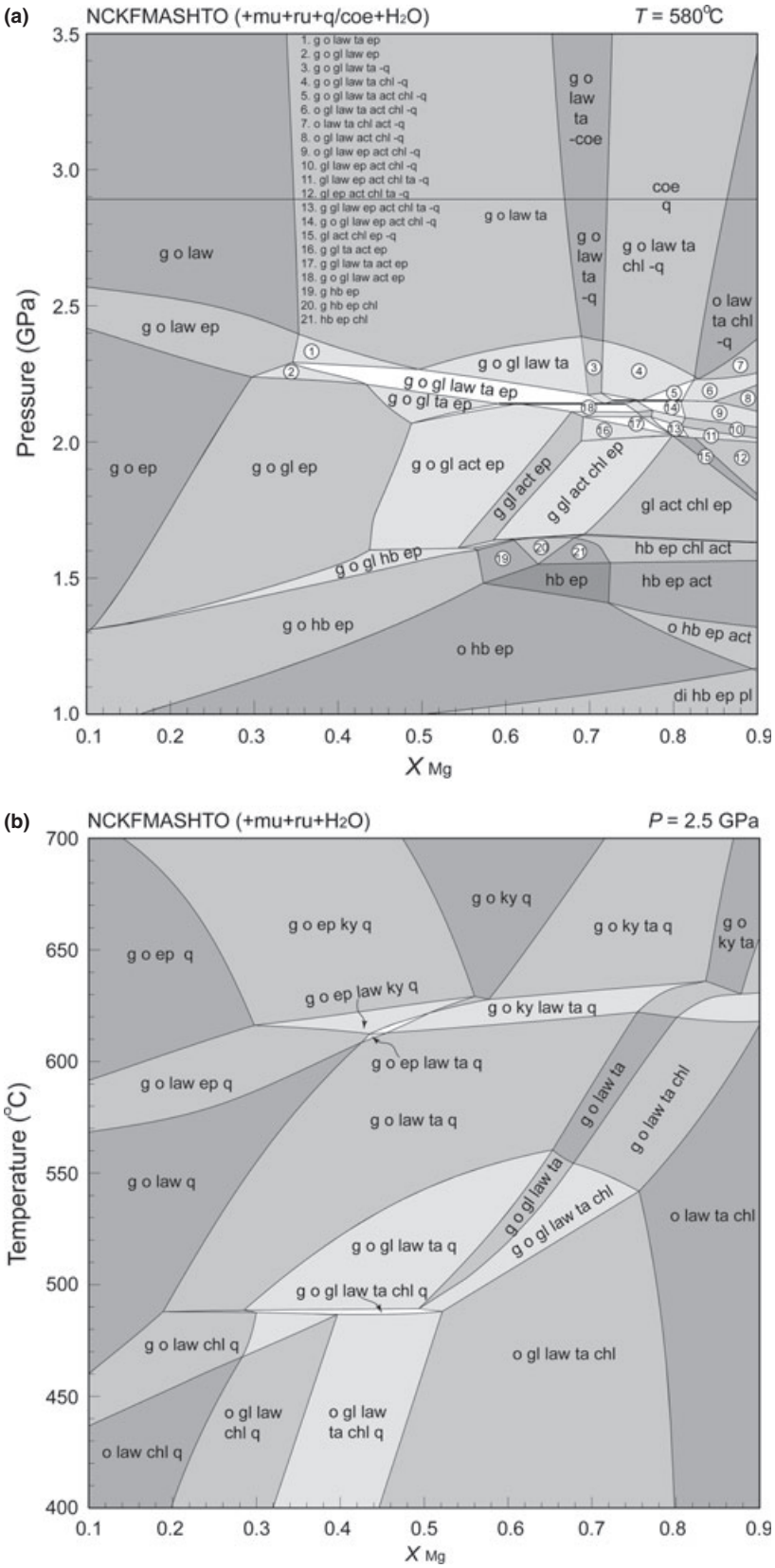

Fig. 7. P–X_{Mg} [= MgO/(MgO + FeO_{tot}), mol.%] pseudosection at 580 °C (a) and T–X_{Mg} pseudosection at 2.5 GPa (b) in the system NCKFMASHTO (+ mu + ru + q/coe + H_2O) for the MORB composition with X_{Mg} = 0.60 in Fig. 3, with the x-axis varying from MgO = 2.04, FeO = 18.33 and O = 2.93 (X_{Mg} = 0.10) to MgO = 18.33, FeO = 2.04 and O = 0.33 (X_{Mg} = 0.90).

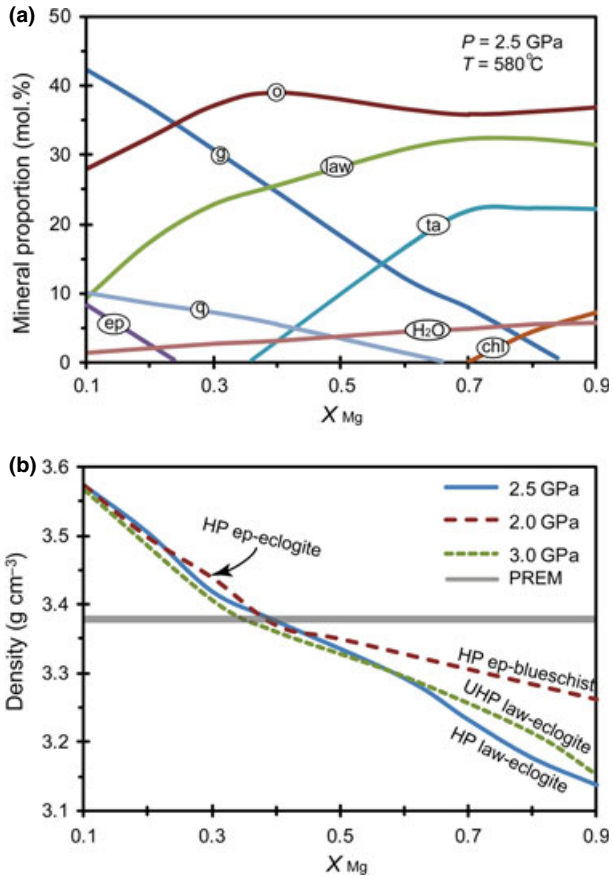

Fig. 8. Calculated mineral proportions at 2.5 GPa, 580 °C (a) and rock densities at 2.0, 2.5 and 3.0 GPa, respectively, (b) with varying bulk-rock X_{Mg} on the basis of Fig. 7a. The H_2O content (wt%) calculated in (a) refers to that just required to saturate the corresponding mineral assemblages. The density of surrounding mantle shown in (b) is 3.37–3.38 g cm^{-3}, based on PREM (Dziewonski & Anderson, 1981).

2.5 GPa and 620 °C corresponding to HP lawsonite–kyanite eclogite; and (5) 2.5 GPa and 650 °C corresponding to HP kyanite eclogite (Fig. 10b). In the lawsonite stability field, increasing X_{Al} changes the density of HP and UHP lawsonite eclogite to lower values (Fig. 10b). At 2.0 GPa and 580 °C, increasing X_{Al} also changes the density of epidote eclogite (with low X_{Al}<0.35) and/or blueschist (with high X_{Al}>0.35) to lower values (Fig. 10b). For the lawsonite–kyanite eclogite (at 2.5 GPa and 620 °C), at X_{Al}<0.30, increasing X_{Al} lowers density; however, at X_{Al}>0.30, X_{Al} has no effect on its density. For the lawsonite-absent kyanite eclogite (at 2.5 GPa and 650 °C), X_{Al} has no effect on its density, as the increase of kyanite with high X_{Al} would buffer the decrease of density.

Bulk-rock X_{Ca}

The natural oceanic eclogites have also a large variation in X_{Ca} [molar ratio of CaO/(CaO + MgO + FeO + Na_2O)] (0.2–0.5) (Table 1). A P–X_{Ca} pseudosection was calculated at 580 °C (Fig. 11a) and a T–X_{Ca} pseudosection at 2.5 GPa (Fig. 11b). Mole proportions of CaO were adjusted with a fixed X_{Mg} (= 0.60) and Fe^{3+}/Fe_{total} (= 0.32), with the x-axis varying from MgO = 15.18, FeO = 10.15, CaO = 7.17, Na_2O = 3.36 and O = 1.62 (X_{Ca} = 0.20) to MgO = 9.49, FeO = 6.34, CaO = 17.93, Na_2O = 2.10 and O = 1.01 (X_{Ca} = 0.50); the mole proportions of other components remains unchanged. The P–X_{Ca} pseudosection shows that increasing X_{Ca} expands the stability of omphacite to lower pressures, At pressures of 1.5–2.4 GPa, the subducted oceanic crust has a blueschist facies (omphacite-absent) assemblage at X_{Ca}<0.32; however, it has an eclogite facies (garnet + omphacite) assemblage at X_{Ca}>0.32. This result is consistent with that of Wei & Clarke (2011). The stability of glaucophane narrows towards higher X_{Ca}, due to the restriction of the g–o–gl–law–ta field in that direction. The stabilities of lawsonite and epidote are not significantly affected by X_{Ca} (Fig. 11a). The T–X_{Ca} pseudosection (Fig. 11b) indicates that kyanite is restricted to high temperatures (>590 °C) in the whole modelled range of X_{Ca}. The increase of X_{Ca} shifts the stability of talc to lower temperatures.

Figure 12a shows the effect of X_{Ca} on mineral proportions in the HP lawsonite eclogite at 2.5 GPa and 580 °C. The increase of X_{Ca} results in a decrease of glaucophane and garnet proportions, and an increase of omphacite, lawsonite and quartz proportions; however, the H_2O content (wt%) required to saturate the corresponding mineral assemblages remains unchanged. Figure 12b illustrates the effect of X_{Ca} on densities of the HP epidote blueschist or HP epidote eclogite (2.0 GPa and 580 °C), HP lawsonite eclogite (2.5 GPa and 580 °C) and UHP lawsonite eclogite (3.0 GPa and 580 °C), and shows that the increase of X_{Ca} increases the densities of HP epidote blueschist and HP epidote eclogite (from 3.19 g cm^{-3} to 3.40 g cm^{-3}), due to the increase in omphacite and epidote proportions. However, the densities of HP lawsonite eclogite and UHP lawsonite eclogite are not significantly affected by X_{Ca}, probably due to the simultaneous increase of lawsonite proportion and decrease of garnet proportion.

Oxidation state

To illustrate the effects of bulk-rock X_{Fe3+} [= $Fe^{3+}/(Fe^{2+} + Fe^{3+})$ = $2O/FeO_{total}$] on mineral assemblage and proportions, a P–X_{Fe3+} pseudosection at 580 °C (Fig. 13) was calculated. Mole proportion of O was adjusted (adjusting X_{Fe3+}), with the x-axis varying from O = 0 at X_{Fe3+} = 0 to O = 3.26 at X_{Fe3+} = 0.8. Figure 13 shows that increasing ferric iron content expands the stability of epidote to higher pressures and that of talc to lower pressures. At <2.0 GPa, omphacite and garnet are not stable in high X_{Fe3+} (>0.24–0.40), and the subducted oceanic crust has blueschist facies assemblages. At X_{Fe3+}<0.24–0.40,

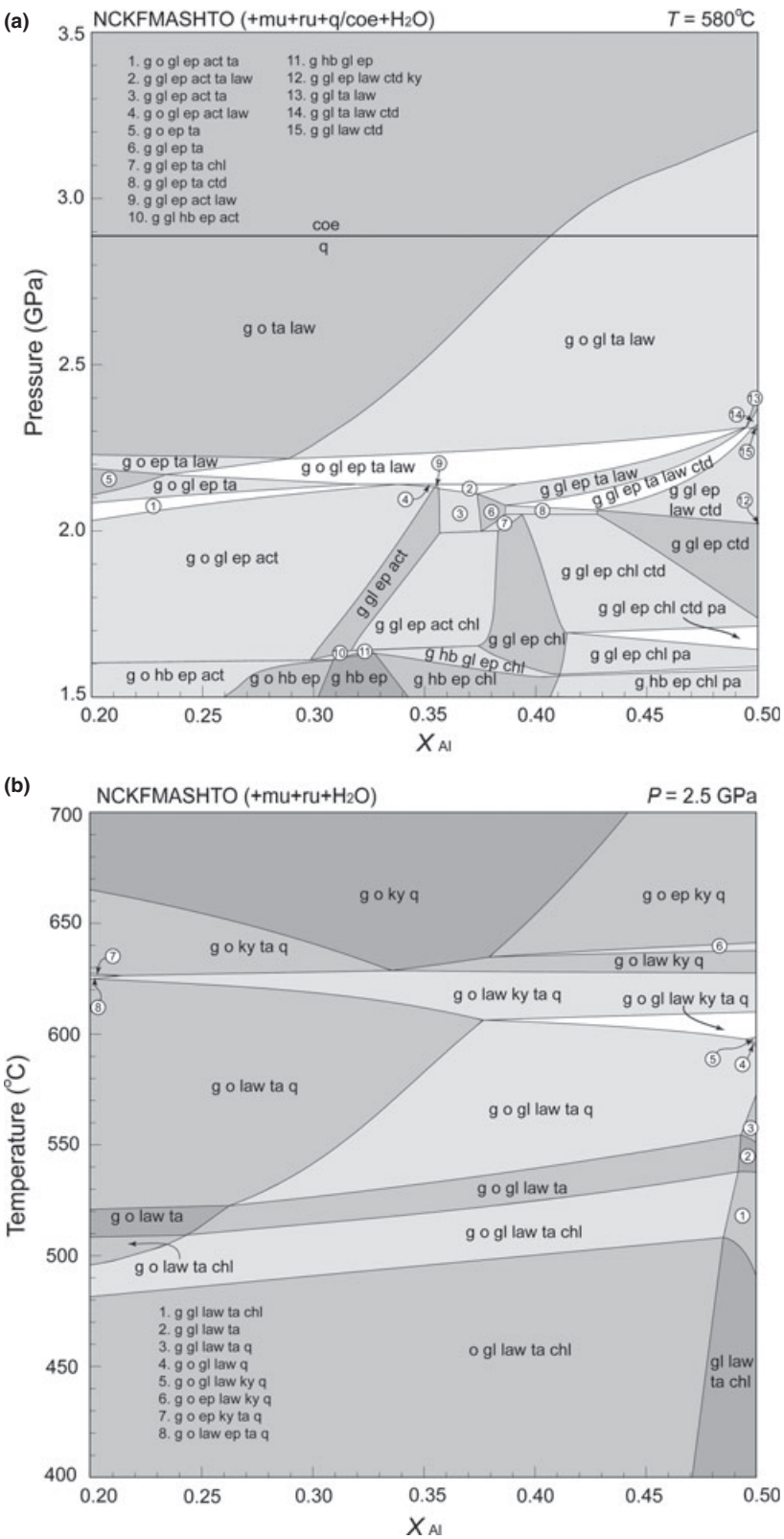

Fig. 9. P–X_{Al} [= Al_2O_3/(Al_2O_3 + MgO + FeO) in mol.%] (a) and T–X_{Al} pseudosections calculated at 580 °C and 2.5 GPa, respectively, using the base composition with X_{Al} = 0.32 in Fig. 3, with the x-axis varying from Al_2O_3 = 6.00, MgO = 14.39, FeO = 9.62 and O = 1.54 (X_{Al} = 0.20) to Al_2O_3 = 15.01, MgO = 9.00, FeO = 6.01 and O = 0.96 (X_{Al} = 0.50).

the subducted oceanic crust has eclogite facies assemblages. Chlorite occurs only in high X_{Fe3+} compositions at pressures lower than 2.1 GPa.

Figure 14a shows the effect of X_{Fe3+} on mineral proportions in the HP lawsonite eclogite at 2.5 GPa and 580 °C. Increasing bulk-rock X_{Fe3+} increases the

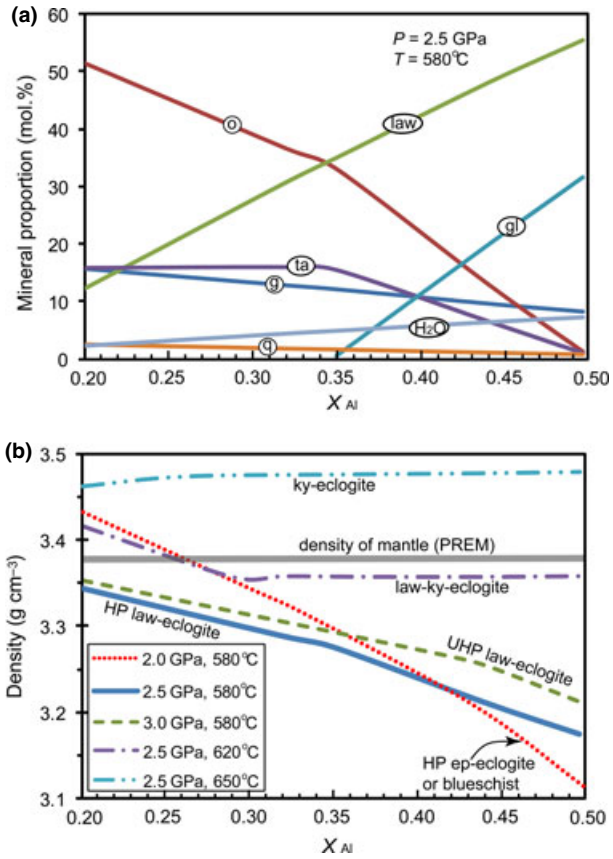

Fig. 10. Calculated mineral proportions at 2.5 GPa, 580 °C (a) and rock densities at 2.0, 2.5 and 3.0 GPa (b) with varying bulk-rock X_{Al} on the basis of Fig. 9a. The rock densities at 2.5 GPa, 620 °C and 2.5 GPa, 650 °C on the basis of Fig. 9b, corresponding to lawsonite–kyanite-bearing and lawsonite-free kyanite-bearing eclogites, are also shown. The H_2O content (wt %) calculated in (a) refers to that just required to saturate the corresponding mineral assemblages. The density of surrounding mantle is after PREM (Dziewonski & Anderson, 1981).

proportions of light lawsonite and talc, but reduces the proportions of dense garnet and omphacite. Figure 14b illustrates the effect of X_{Fe3+} on densities of the HP epidote blueschist or HP epidote eclogite (2.0 GPa and 580 °C), HP lawsonite eclogite (2.5 GPa and 580 °C) and UHP lawsonite eclogite (3.0 GPa and 580 °C). The increase of X_{Fe3+} decreases the density of all rocks types (Fig. 14b).

DISCUSSION AND CONCLUSIONS

Depth limitation for the exhumation of oceanic eclogites

The exhumation of deep subducted HP–UHP crustal rocks is widely considered driven by buoyancy forces (Davies & von Blanckenburg, 1995; Ernst *et al.*, 1997; Ernst, 2001, 2005, 2006; Guillot *et al.*, 2009); once decoupled from the down-going slab, the HP–UHP rocks with densities lower than the surrounding mantle are expected to be exhumed to crustal levels (Ernst, 2001, 2006). The density profile derived from the Preliminary Reference Earth Model (PREM) (Dziewonski & Anderson, 1981) is commonly used to represent the density evolution of mantle as a function of depth (e.g. Aoki & Takahashi, 2004; Hirose *et al.*, 2005; Litasov & Ohtani, 2005; Perrillat *et al.*, 2006; Wu *et al.*, 2009). Therefore, a comparison of the density of subducted HP–UHP crustal rocks and PREM can provide constraints on the critical depth where subducted oceanic crust becomes neutrally buoyant with respect to the surrounding mantle. For example, because the coesite-bearing felsic continental crust is less dense than the surrounding mantle at <7.5 GPa, deeply subducted UHP upper continental crust at depths of < ~250 km has the potential to be uplifted by buoyancy (Wu *et al.*, 2009). This viewpoint is widely used to interpret the common exhumation of the worldwide HP–UHP terranes formed by the subduction of upper continental crust (Davies & von Blanckenburg, 1995; Ernst, 2001; Wu *et al.*, 2009; Zhao *et al.*, 2011).

A similar comparison can also be used to constrain the exhumation of oceanic eclogites. Our modelling demonstrates that, along the cold subduction P–T path (6 °C km^{-1} geothermal gradient), the density of the cold and hydrous oceanic eclogites is always less than that of the surrounding mantle at depths of < ~110 km (Fig. 4c). Therefore, it is reasonable to predict that such cold and hydrous oceanic eclogites at depths shallower than 110 km can be exhumed back to the crustal level, driven by the buoyancy force, and that those at depths greater than 110 km would sink into deeper mantle. However, our modelling results also demonstrate that, along the warm subduction P–T path (~10 °C km^{-1} geothermal gradient), the subducted MORB is transformed to hot and dry eclogites at pressures of > ~1.9 GPa (Figs 3 & 4b); as a result, it becomes denser than the surrounding mantle at depths > ~60 km (Fig. 4c).

The densities of all of the oceanic eclogites formed at various geothermal gradients can be calculated by the methods employed in this study. Furthermore, by knowing these densities, we can find a curve for the return depth limit for the oceanic eclogites formed at various geothermal gradients (Fig. 1). Our modelling results suggest that only the oceanic eclogites formed at the P–T regions on the left side of the depth limit curve have lower densities than the surrounding mantle. Figure 1 shows that all of the exhumed oceanic eclogites in oceanic subduction zones are located within our predicted exhumation P–T regions. Because the geothermal gradients of the realistic subducted oceanic slabs are commonly assumed to be higher than 5 °C km^{-1} (e.g. Agard *et al.*, 2009; Brovarone *et al.*, 2011; Endo *et al.*, 2012), our modelling results indicate that the maximum exhumation depth for oceanic eclogites may be

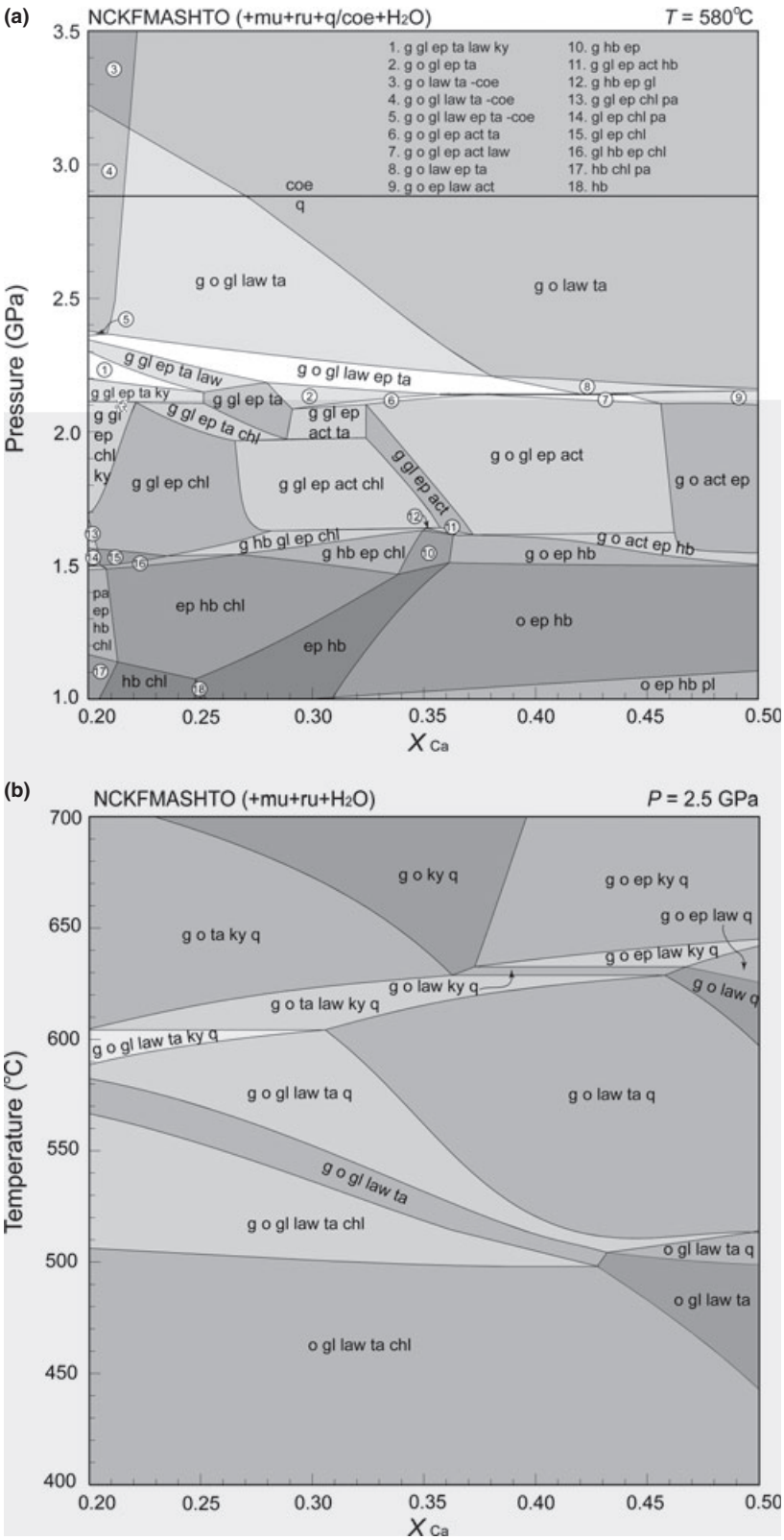

Fig. 11. P–X_{Ca} [= CaO/(CaO + MgO + FeO + Na_2O)] (a) and T–X_{Ca} (b) pseudosections for 580 °C and 2.5 GPa, respectively, for the base composition with X_{Ca} = 0.36 in Fig. 3, with the x-axis varying from MgO = 15.18, FeO = 10.15, CaO = 7.17, Na_2O = 3.36 and O = 1.62 (X_{Ca} = 0.20) to MgO = 9.49, FeO = 6.34, CaO = 17.93, Na_2O = 2.10 and O = 1.01 (X_{Ca} = 0.50).

<120 km (<3.6 GPa) (Fig. 1). This constraint is consistent with the fact that all of the exhumed oceanic eclogites in natural oceanic subduction zones are cold and hydrous eclogites and that their maximum formation depth is <110 km (Fig. 1) (Green, 2005; Agard *et al.*, 2009). The cold and hydrous UHP

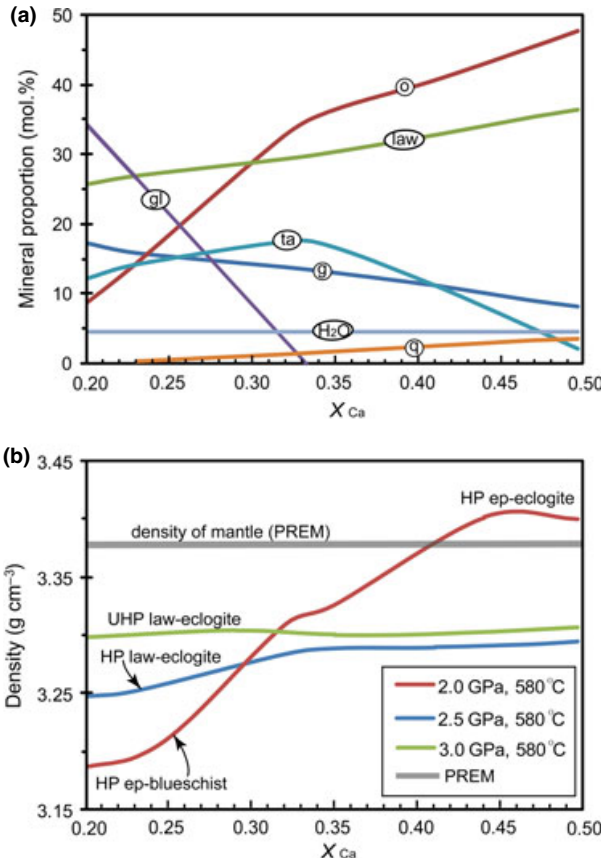

Fig. 12. Calculated mineral proportions at 2.5 GPa, 580 °C (a) and rock densities at 2.0, 2.5 and 3.0 GPa (b), respectively, with varying bulk-rock X_{Ca} on the basis of Fig. 11a. The H_2O content (wt%) calculated in (a) refers to that just required to saturate the corresponding mineral assemblages. The density of surrounding mantle is after PREM (Dziewonski & Anderson, 1981).

lawsonite-bearing oceanic eclogites formed at depths greater than 110–120 km along a geothermal gradient of < ~7 °C km^{-1} are denser than the surrounding mantle (Fig. 1), and they are therefore expected to sink into deeper mantle. The lawsonite-bearing eclogite xenoliths in kimberlitic pipes from the Colorado Plateau (Usui *et al.*, 2003, 2006) may be representative of such sinking cold and hydrous lawsonite eclogites. Such eclogites can carry a large amount of H_2O into the mantle at depths of up to 300 km (Schmidt & Poli, 1998; Okamoto & Maruyama, 1999). Our modelling results also indicate that all of the hot and dry oceanic eclogites predicted in the pseudosection calculations (e.g. those formed at depths >60 km (>1.8 GPa) along the 10 °C km^{-1} geothermal gradient, Fig. 4c) are denser than the surrounding mantle (Fig. 1), and we thus predict that they cannot be exhumed and that they are expected to sink into deeper mantle. This prediction is consistent with the fact that no hot–dry oceanic eclogites have been found in the natural oceanic subduction zones (Fig. 1). Dense, hot and dry oceanic crust is commonly suggested by geophysical observations in transition zones (Zhao *et al.*, 2007; Zhao, 2008), the lower mantle (Fukao *et al.*, 2001), and even the core–mantle boundary (Hirose *et al.*, 1999; Karason & van der Hilst, 2000).

Effect of bulk-rock composition on the exhumation of oceanic eclogites

Based on the calculation results presented above, the phase relations and densities of subducted oceanic crusts are also affected by bulk-rock composition; thus, it is important to determine the effect of bulk-rock composition on the exhumation of oceanic eclogites.

Our study indicates that the densities of oceanic eclogites are affected by the bulk-rock X_{Mg}, X_{Al} and X_{Ca} (Figs 8, 10 & 12). Our modelling suggests that the oceanic eclogites most likely to undergo exhumation are approximately constrained to have compositions of high-Mg (X_{Mg}>0.40, Fig. 8), high-Al (X_{Al}>0.26, Fig. 10), and low-Ca (X_{Ca}<0.41, Fig. 12). However, the bulk-rock X_{Ca} does exert a significant effect on the exhumation of HP and UHP lawsonite eclogites (Fig. 12). Figure 15 shows X_{Mg}–X_{Al} and X_{Mg}–X_{Ca} plots of the bulk-rock compositions of the exhumed oceanic eclogites worldwide reported in the literature (see Table 1 and references therein), most (>90%) plot in the shaded fields constrained by our calculations, consistent with our bulk-rock compositional constraints for the exhumation of oceanic eclogites. It is worth noting that the eclogite samples with high X_{Ca} exceeding the constrained compositional range (Fig. 15b) are all lawsonite eclogites whose densities are not significantly affected by X_{Ca} (Fig. 12).

Figure 6 shows that only the oceanic eclogites with moderately high H_2O contents have densities lower than that of the surrounding mantle, and we thus predict that only H_2O-rich oceanic eclogites can be exhumed to a crustal level. The required H_2O contents for the exhumation of oceanic eclogites formed under various pressure conditions at 580 °C (Fig. 6) are ~ >1.2 wt% for HP epidote eclogites, >2.3 wt% for HP lawsonite eclogites and >3.3 wt% for UHP lawsonite eclogites. The predicted H_2O values match well with H_2O contents of natural oceanic eclogites. The predicted H_2O values for HP epidote eclogites (>1.2 wt%) are consistent with those of epidote eclogites from the Sivrihisar Massif in Turkey (1.44 wt%, Davis & Whitney, 2006) and in the Adean Raspas Complex in Ecuador (1.38 wt%, Bosch *et al.*, 2002); the predicted H_2O values for HP and UHP lawsonite eclogites (>2.3 wt%) are consistent with those for lawsonite eclogites in Alpine Corsica (5.12–5.23 wt%, Brovarone *et al.*, 2011) and in the Sivrihisar Massif in Turkey (3.13 wt%, Davis & Whitney, 2006). Further considering the high proportions of peak hydrous minerals (25–75 vol%) in oce-

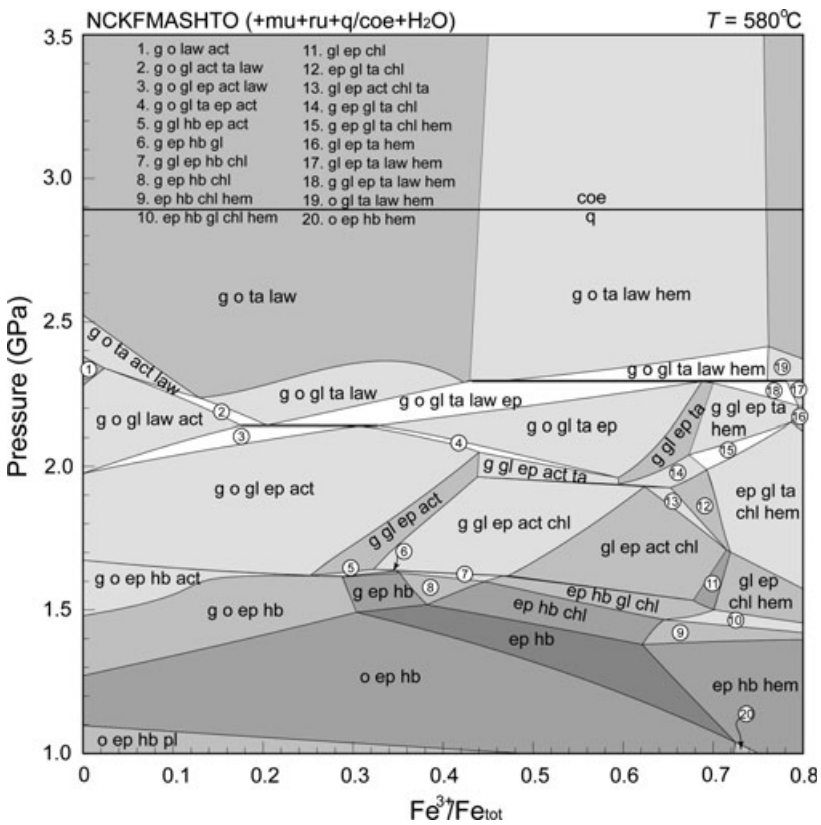

Fig. 13. P–X_{Fe3+} [== $Fe^{3+}/(Fe^{2+} + Fe^{3+}) = 2O/FeO_{total}$] pseudosection at 580 °C, using the base composition given in Fig. 3, with O = 0 at $X_{Fe3+} = 0$, and O = 3.26 at $X_{Fe3+} = 0.8$.

anic eclogites (e.g. Davis & Whitney, 2006; Ghent *et al*., 2009; Wei *et al*., 2009a), and good consistency between thermodynamic modelling results in H_2O-saturated systems and petrological observations in natural samples (e.g. Groppo & Castelli, 2010; Brovarone *et al*., 2011; Angiboust *et al*., 2012; Endo *et al*., 2012), we regard that the exhumed oceanic eclogites really have moderately high H_2O content. Prior to subduction, H_2O content will correspond to what is capable of being produced by hydrothermal metamorphism at spreading centres. During subduction, the access of H_2O may be derived from dehydration of associated subducted metasedimentary rocks (e.g. Clarke *et al*., 2006) or serpentinites beneath the subducted oceanic crust (e.g. Spandler *et al*., 2011).

Figure 14 clearly shows that high X_{Fe3+} (at least >0.1 for lawsonite eclogite) will favour the exhumation of oceanic crust. To date, the oxidation state of subducted oceanic crust has not been well constrained; however, it is highly likely that the oxidation state is intermediate to high for subducted oceanic crust. Eclogites from various subduction zones and ages commonly have higher X_{Fe3+} than unaltered MORB samples (0.12–0.16) (e.g. Bezos & Humler, 2005; Groppo & Castelli, 2010; Kabir & Takasu, 2010; Rebay *et al*., 2010; Cottrell & Kelley, 2011; Endo *et al*., 2012). In addition, the oxygen fugacity of subducted oceanic crust would increase during ductile deformation associated with exhumation (e.g. North Qilian lawsonite eclogite, Cao *et al*., 2011), which may in turn promote the exhumation of oceanic eclogites.

Role of associated blueschists on the exhumation of oceanic eclogites

Oceanic eclogites are commonly associated with serpentinites, metasediments, and blueschist facies metabasites. Some previous studies (Hermann *et al*., 2000; Guillot *et al*., 2001, 2009; Schwartz *et al*., 2001; Wei & Song, 2008; Wei *et al*., 2009b) suggested that the exhumation of oceanic crust was probably facilitated by their association with serpentinites and metasediments, which would counterbalance their negative buoyancy and enhance mechanical decoupling. Our modelling suggests that blueschists would also potentially enhance mechanical decoupling and promote the exhumation of oceanic eclogites at depth of <100 km.

The coexistence of blueschist and eclogite is a very common phenomenon in oceanic subduction zones. The development of blueschists is previously considered prograde or retrograde products of the associated eclogites (e.g. Carson *et al*., 2000). Recent thermodynamic studies revealed that oceanic low-T eclogite and blueschist may experience a similar P–T evolution but with different bulk-rock X_{Ca} or fluid activities (Brovarone *et al*., 2011; Wei & Clarke,

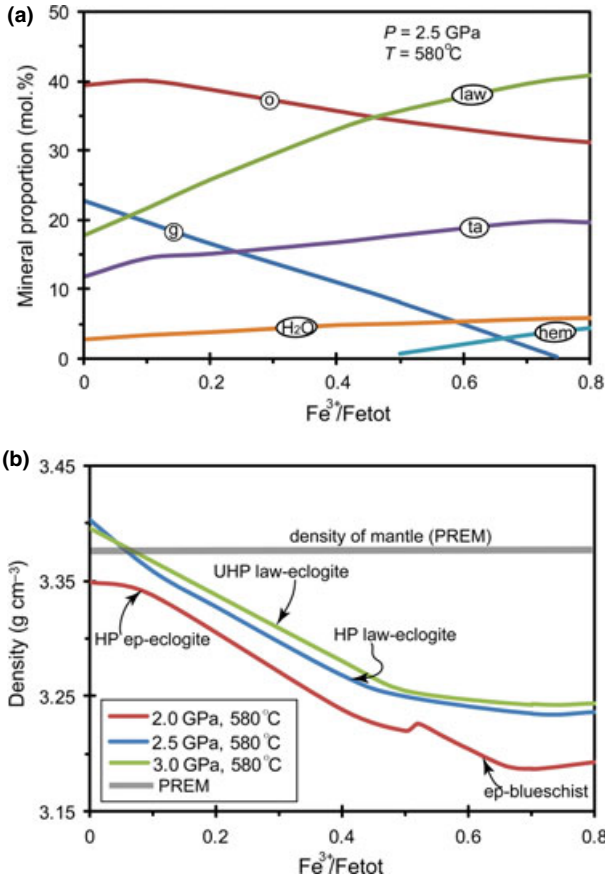

Fig. 14. Calculated mineral proportions at 2.5 GPa, 580 °C (a) and rock densities at 2.0, 2.5 and 3.0 GPa (b), respectively, with varying bulk-rock X_{Fe3+} on the basis of Fig. 13. The density of surrounding mantle is after PREM (Dziewonski & Anderson, 1981). The H_2O content (wt%) calculated in (a) refers to that just required to saturate the corresponding mineral assemblages.

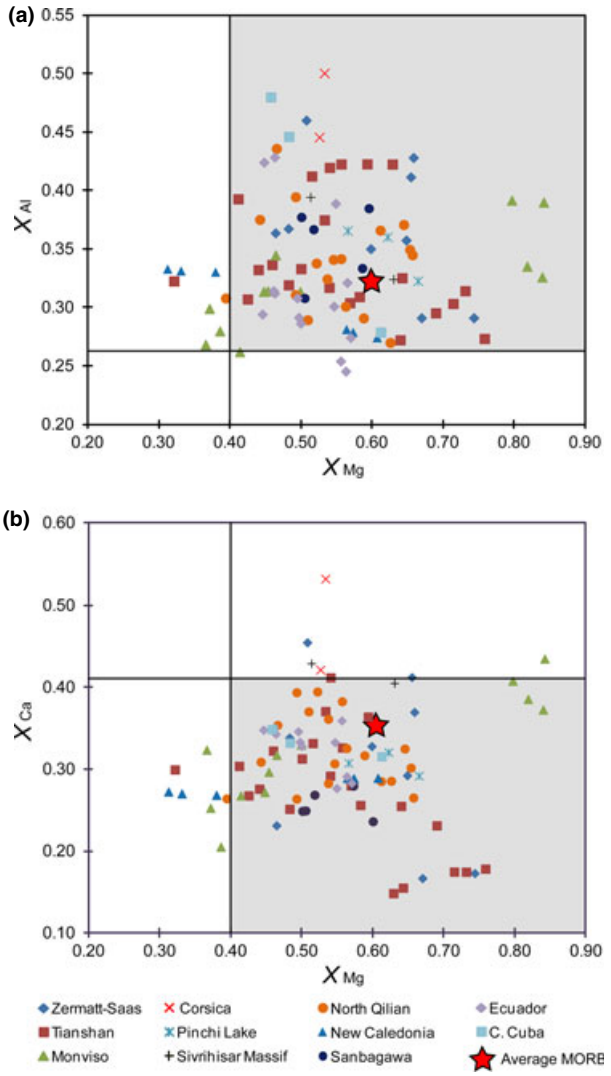

Fig. 15. X_{Mg}–X_{Al} (a) and X_{Mg}–X_{Ca} (b) plots of the bulk-rock compositions of the exhumed oceanic eclogites worldwide reported in the literature listed in Table 1. The shaded fields represent the bulk-rock compositional constraints for the exhumation of oceanic eclogites in this study. The average MORB composition used in Fig. 3 is also shown.

2011). Beside bulk-rock X_{Ca}, our calculations indicate that the coexistence of eclogite and blueschist can also result from different bulk-rock X_{Mg}, X_{Al} and X_{Fe3+} at the same P–T conditions. As shown in Figs 7a, 9a & 13, lawsonite- or epidote-bearing eclogites may form in bulk compositions involving lower X_{Mg} (<0.70), X_{Al} (<0.35) and X_{Fe3+} (<0.40), respectively, whereas lawsonite- or epidote-bearing blueschists may occur as a result of bulk compositions involving higher X_{Mg} (>0.54), X_{Al} (>0.35), and X_{Fe3+} (>0.24). This observation is supported by the coexistence of the epidote-bearing eclogite and blueschist in the Pam Peninsula, New Caledonia (Fitzherbert *et al.*, 2003), where the eclogite has lower X_{Mg} = 0.31, and the blueschist has higher X_{Mg} = 0.61. Petrological observations and thermodynamic modelling imply that they share similar P–T evolution (Fitzherbert *et al.*, 2003). At 580 °C, the blueschist facies assemblages are commonly restricted to be lower pressures of <2.5 GPa (Figs 7a, 9a, 11a & 13); however, they can be also stable at higher pressures up to 3.0 GPa for lower temperatures (e.g. 500 °C) with extremely low X_{Ca}<0.20 (Wei & Clarke, 2011). Even though blueschist and eclogite may share similar P–T evolutions, the physical properties of these two types of rocks are quite different. Figures 8, 10, 12 and 14 show that the density of epidote blueschist is systematically lower than that of epidote eclogite at the same P–T conditions, the density discrepancy can be up to 0.3–0.4 g cm^{-3}. Therefore, low-density blueschists would also enhance mechanical decoupling and promote exhumation of oceanic eclogites along the subduction channel.

On the basis of above constraints, we therefore suggest that beyond maximum depths of ~110–

120 km there are no blueschists and/or the oceanic eclogites are not light enough to compensate the negative buoyancy of the oceanic crust. This depth limitation is consistent with the fact that no oceanic eclogites, returned from ultradeep mantle (>120 km) to the surface, have been found in oceanic subduction zones (Green, 2005; Agard *et al*., 2009).

Detachment of light–cold–hydrous eclogites from the sinking slab

As previously reviewed, almost all natural oceanic eclogites found to have been exhumed from oceanic subduction zones are light–cold–hydrous eclogites (Fig. 1) (e.g. Zack *et al*., 2004; Lü *et al*., 2009; Wei *et al*., 2009a; Angiboust & Agard, 2010; Brovarone *et al*., 2011; Zhai *et al*., 2011; Angiboust *et al*., 2012; Plunder *et al*., 2012), and dense–hot–dry oceanic eclogites are lacking even in typical warm oceanic subduction zones, such as in SW Japan (Tsujimori & Matsumoto, 2006) and the Sanbagawa belt (Wallis *et al*., 2000; Kabir & Takasu, 2010). This result suggests that exhumed light–cold–hydrous oceanic eclogites must have detached from the denser oceanic eclogites, which are expected to sink into deeper mantle.

Our modelling results demonstrate that the calculated buoyancy of eclogites in the mantle is strongly dependent on the proportion of light hydrous phases which is controlled by H_2O content. It is commonly assumed that the top parts of subducted oceanic crust are altered basalts with high H_2O content, whereas the bottom parts are gabbro with low H_2O content. Therefore, most of natural light–cold–hydrous oceanic eclogites are very likely to originate from the top parts of subducted oceanic crust. This is further supported by the fact that the natural oceanic eclogites are usually associated with metasediments (Wei *et al*., 2009b; Klemd *et al*., 2011) or wedge serpentinites (Guillot *et al*., 2001, 2009). Numerical calculations demonstrate that, at depths beneath the arc, temperatures at the top of subducted crust are as high as 650–1000 °C (Syracuse *et al*., 2010; van Keken *et al*., 2011). Therefore, the top part of subducted oceanic crust should be transformed to dense–hot eclogites at sub-arc depths (Figs 3 & 4b), it is denser than the surrounding mantle (Fig. 4c) and no light serpentinites can survive in this region (Fig. 16). This conclusion is also supported by recent thermodynamic modelling of global subduction slabs (van Keken *et al*., 2011). Several recent studies (Federico *et al*., 2007; Krebs *et al*., 2008; Blanco-Quintero *et al*., 2010; Malatesta *et al*., 2012) demonstrated that there was a return channel flow which is driven by mass conservation in the serpentinized subduction channel. At shallow depths in the forearc region (<110–120 km), cold–hydrous eclogites with high Mg, Al, Fe^{3+} and H_2O and low Ca are lighter than the mantle, and serpentinites can be stable in the subduction channel (Fig. 16). We suggest that the cold–hydrous eclogites and blueschists are scraped off from the top of the subducting slab at shallow depths in the forearc region (<110–120 km) and are exhumed inside serpentinized subduction channels (Gerya *et al*., 2002; Gorczyk *et al*., 2007; Guillot *et al*., 2009; Malatesta *et al*., 2012). The dense–hot eclogites formed at depths under the arc are denser than the mantle and thus have no chance to return to the surface.

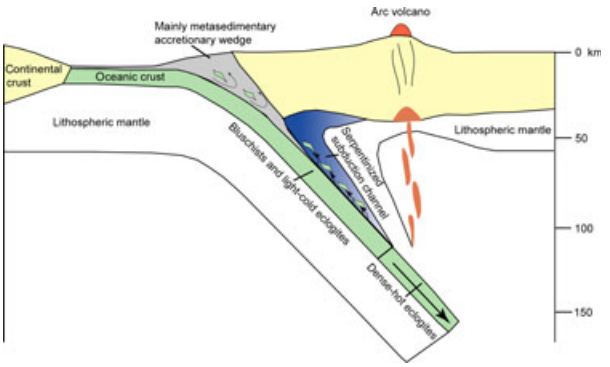

Fig. 16. Schematic model for the exhumation of oceanic eclogites (and blueschists) in a cold oceanic subduction zone (modified after Guillot *et al*., 2009). In the forearc region (<110–120 km), the light blueschists and cold-hydrous eclogites (and also metasediments) are detached from the top of the subducting slab and are exhumed inside serpentinized subduction channel by return channel flow (Gerya *et al*., 2002; Gorczyk *et al*., 2007; Guillot *et al*., 2009; Malatesta *et al*., 2012). The dense-hot eclogites formed at greater depth (e.g. beneath the arc) are denser than the mantle and thus are expected to sink into deeper mantle.

ACKNOWLEDGEMENTS

This study is financially supported by the National Basic Research Program of China (973 Program 2009CB825001) and the National Science Foundation of China (No. 40902023, 41090371, 40922150, 41023009). This study has benefited from discussions with Dr. Y. Wu. Profs T. V. Gerya and C. J. Wei, and Dr. E. Green are thanked for their critical reviews on the manuscript. Prof. R. White is much appreciated for his detailed editorial work.

REFERENCES

Agard, P., Yamato, P., Jolivet, L. & Burov, E., 2009. Exhumation of oceanic blueschists and eclogites in subduction zones: timing and mechanisms. *Earth Science Reviews*, **92,** 53–79.

Altherr, R., Topuz, G., Marschall, H., Zack, T. & Ludwig, T., 2004. Evolution of a tourmaline-bearing lawsonite eclogite from the Elekdag area (Central Pontides, N Turkey): evidence for infiltration of slab-derived B-rich fluids during exhumation. *Contributions to Mineralogy and Petrology*, **148,** 409–425.

Angiboust, S. & Agard, P., 2010. Initial water budget: the key to detaching large volumes of eclogitized oceanic crust along the subduction channel? *Lithos*, **120,** 453–474.

Angiboust, S., Langdon, R., Agard, P., Waters, D. & Chopin, C., 2012. Eclogitization of the Monviso ophiolite (W. Alps) and implications on subduction dynamics. *Journal of Metamorphic Geology*, **30,** 37–61.

Aoki, I. & Takahashi, I., 2004. Density of MORB eclogite in the upper mantle. *Physics of the Earth and Planetary Interiors*, **143,** 129–143.

Bezos, A. & Humler, E., 2005. The $Fe^{3+}/\sum Fe$ ratios of MORB glasses and their implications for mantle melting. *Geochimica et Cosmochimica Acta*, **69,** 711–725.

Blanco-Quintero, I.F., García-Casco, A. & Gerya, T.V., 2010. Tectonic blocks in serpentinite mélange (eastern Cuba) reveal large-scale convective flow of the subduction channel. *Geology*, **39,** 79–82.

Bosch, D., Gabriele, P., Lapierre, H., Malfere, J.L. & Jaillard, E., 2002. Geodynamic siginificance of the Raspas Metamorphic Complex (SW Ecuador): geochemical and isotopic constraints. *Tectonophysics*, **345,** 83–102.

Brovarone, A.V., Groppo, C., Hetanyi, G., Compagnoni, R. & Malavieille, J., 2011. Coexistence of lawsonite-bearing eclogite and blueschist: phase equilibria modelling of Alpine Corsica metabasalts and petrological evolution of subducting slabs. *Journal of Metamorphic Geology*, **29,** 583–600.

Cao, Y., Song, S.G., Niu, Y.L. & Jin, Z.M., 2011. Variation of mineral composition, fabric and oxygen fugacity from massive to foliated eclogites during exhumation of subducted ocean crust in the North Qilian suture zone, NW China. *Journal of Metamorphic Geology*, **29,** 699–720.

Carson, C.J., Clarke, G.L. & Powell, R., 2000. Hydration of eclogite, Pam Peninsula, New Caledonia. *Journal of Metamorphic Geology*, **18,** 79–90.

Clarke, G.L., Aitchison, J.C. & Cluzel, D., 1997. Eclogites and blueschists of the Pam Peninsula, NE New Caledonia: a reappraisal. *Journal of Petrology*, **38,** 843–876.

Clarke, G.L., Powell, R. & Fitzherbert, J.A., 2006. The lawsonite paradox: mineral equilibria modelling in the system Na_2O-CaO-K_2O-FeO-MgO-Al_2O_3-SiO_2-H_2O. *Journal of Metamorphic Geology*, **24,** 715–725.

Coggon, R. & Holland, T.J.B., 2002. Mixing properties of phengitic micas and revised garnet–phengite thermobarometers. *Journal of Metamorphic Geology*, **20,** 683–696.

Connolly, J.A.D., 1990. Multivariable phase diagrams: an algorithm based on generalized thermodynamics. *American Journal of Science*, **290,** 666–718.

Cottrell, E. & Kelley, K.A., 2011. The oxidation state of Fe in MORB glasses and the oxygen fugacity of the upper mantle. *Earth and Planetary Science Letters*, **305,** 270–282.

Davies, J.H. & von Blanckenburg, F., 1995. Slab breakoff: a model of lithosphere detachment and its test in the magmatism and deformation of collisional orogens. *Earth and Planetary Science Letters*, **129,** 85–102.

Davis, P.B. & Whitney, D.L., 2006. Petrogenesis of lawsonite an epidote eclogite and blueschist, Sivrihisar Massif, Turkey. *Journal of Metamorphic Geology*, **24,** 823–849.

Davoudian, A.R., Genser, J., Dachs, E. & Shabanian, N., 2008. Petrology of eclogites from north of Shahrekord, Sanandaj-Sirjan Zone, Iran. *Mineralogy and Petrology*, **92,** 393–413.

Diener, J.F.A., Powell, R., White, R.W. & Holland, T.J.B., 2007. A new thermodynamic model for clino- and orthoamphiboles in the system Na_2O-CaO-FeO-MgO-Al_2O_3-SiO_2-H_2O-O. *Journal of Metamorphic Geology*, **25,** 631–656.

Dziewonski, A.M. & Anderson, D.L., 1981. Preliminary reference Earth model. *Physics of the Earth and Planetary Interiors*, **25,** 297–356.

Endo, S., Wallis, S.R., Tsuboi, M., Torres, R. & Solari, L.A., 2012. Metamorphic evolution of lawsonite eclogites from the southern Motagua fault zone, Guatemala: insights from phase equilibria and Raman spectroscopy. *Journal of Metamorphic Geology*, **30,** 143–164.

Ernst, W.G., 2001. Ultra-high pressure metamorphism, and regurgitation of buoyant crustal slices: implications for arcs and continental growth. *Physics of the Earth and Planetary Interiors*, **127,** 253–275.

Ernst, W.G., 2005. Alpine and Pacific styles of Phanerozic mountain building: subduction-zone petrogenesis of continental crust. *Terra Nova*, **17,** 165–188.

Ernst, W.G., 2006. Preservation/exhumation of ultrahigh-pressure subduction complexes. *Lithos*, **92,** 321–335.

Ernst, W.G., Maruyama, S. & Walis, S.R., 1997. Buoyancy-driven, rapid exhumation of ultrahigh-pressure metamorphosed continental crust. *Proceedings of the National Academy of Sciences*, **94,** 9532–9537.

Federico, L., Capponi, G., Crispini, L. & Scambelluri, M., 2004. Exhumation of alpine high-pressure rocks: insights from petrology of eclogite clasts in the Tertiary Piedmontese basin (Ligurian Alps, Italy). *Lithos*, **74,** 21–40.

Federico, L., Crispini, L., Scambelluri, M. & Capponi, G., 2007. Ophiolite mélange zone records exhumation in a fossil subduction channel. *Geology*, **35,** 499–502.

Fitzherbert, J.A., Clarke, G.L. & Powell, R., 2003. Lawsonite-omphacite-bearing metabasites of the Pan Peninsula, NE New Caledonia: evidence for disrupted blueschist-to eclogite-facies conditions. *Journal of Petrology*, **44,** 1805–1831.

Forneris, J.F. & Holloway, J.R., 2003. Phase equilibria in subducting basaltic crust: implications for H_2O release from the slab. *Earth and Planetary Science Letters*, **214,** 187–201.

Fotoohi Rad, G.R., Droop, G.T.R., Amini, S. & Moazzen, M., 2005. Eclogites and blueschists of the Sistan Suture Zone, eastern Iran: a comparison of P-T histories from a subduction mélange. *Lithos*, **84,** 1–24.

Fukao, Y., Widiyantoro, S. & Obayashi, M., 2001. Stagnant slabs in the upper and lower mantle transition zone. *Reviews of Geophysics*, **39,** 291–323.

Gao, J., John, T., Klemd, R. & Xiong, X.M., 2007. Mobilization of Ti-Nb-Ta during subduction: evidence from rutile-bearing dehydration segregations and veins hosted in eclogite, Tianshan, NW China. *Geochimica Cosmochimica Acta*, **71,** 4974–4996.

García-Casco, A., Torres-Roldan, R.L., Millan, G. & Schneider, J., 2002. Oscillatory zoning in eclogitic garnet and amphibole, Northern Serpentinite Mélange, Cuba: a record of tectonic instability during subduction? *Journal of Metamorphic Geology*, **20,** 581–598.

García-Casco, A., Torres-Roldan, R.L., Iturralde-Vinent, M.A. *et al*., 2006. High pressure metamorphism of ophiolites in Cuba. *Geological Acta*, **4,** 63–88.

Gerya, T.V., Stoeckhert, B. & Perchuk, A.L., 2002. Exhumation of high-pressure metamorphic rocks in a subduction channel – a numerical simulation. *Tectonics*, **21,** 1056. doi:10.1029/2002TC001406.

Ghent, E., Tinkham, D. & Marr, R., 2009. Lawsonite eclogites from the Pinchi Lake area, British Columbia-new P-T estimates and interpretation. *Lithos*, **109,** 248–253.

Gorczyk, W., Guillot, S., Gerya, T.V. & Hattori, K., 2007. Asthenospheric upwelling, oceanic slab retreat and exhumation of UHP mantle rocks: insights from Greater Antilles. *Geophysical Research Letters*, **34,** L211309. doi:10.1029/2007GL031059.

Green, H.W.I., 2005. Psychology of a changing paradigm: 40+ years of high-pressure metamorphism. *International Geology Review*, **47,** 439–456.

Green, E.C.R., Holland, T.J.B. & Powell, R., 2007. An order–disorder model for omphacitic pyroxenes in the system jadeite–diopside–hedenbergite–acmite, with applications to eclogitic rocks. *American Mineralogists*, **92,** 1181–1189.

Groppo, C. & Castelli, D., 2010. Prograde P-T evolution of a lawsonite eclogite from the Monviso meta-ophiolite (Western Alps): dehydration and redox reactions during subduction of oceanic FeTi-oxide gabbro. *Journal of Petrology*, **51,** 2489–2514.

Groppo, C., Beltrando, M. & Compagnoni, R., 2009. The P-T path of the ultra-high pressure Lago Di Cignana and adjoining high-pressure meta-ophiolitic units: insights into the evolution of the subducting Tethyan slab. *Journal of Metamorphic Geology*, **27,** 207–231.

Guillot, S., Hattori, K.H., Sigoyer, J., Nagler, T. & Auzende, A-.L., 2001. Evidence of hydration of the mantle wedge and

its role in the exhumation of eclogites. *Earth and Planetary Science Letters*, **193,** 115–127.
Guillot, S., Hattori, K., Agard, P., Schwartz, S. & Vidal, O., 2009. Exhumation processes in oceanic and continental subduction contexts: a review, subduction zone geodynamics. *Frontiers in Earth Sciences*. Springer, Berlin Heidelberg, pp. 175–205.
Hacker, B.R., Abers, G.A. & Peacock, S.M., 2003. Subduction factory 1. Theoretical mineralogy, densities, seismic wave speeds, and H_2O contents. *Journal of Geophysical Research*, **108**, doi:10.1029/2001JB001127.
Hermann, J., Muntener, O. & Scambelluri, M., 2000. The importance of serpentinite mylonites for subduction and exhumation of oceanic crust. *Tectonophysics*, **217,** 225–238.
Hirose, K., Fei, Y., Ma, Y. & Mao, H.-K., 1999. The fate of the subducted basaltic crust in the Earth's lower mantle. *Nature*, **397,** 53–56.
Hirose, K., Takafuji, N., Sata, N. & Ohishi, Y., 2005. Phase transition and density of subducted MORB crust in the lower mantle. *Physics of the Earth and Planetary Interiors*, **237,** 139–151.
Holland, T.J.B. & Powell, R., 1998. An internally consistent thermodynamic data set for phases of petrological interest. *Journal of Metamorphic Geology*, **16,** 309–343.
Holland, T.J.B. & Powell, R., 2003. Activity-composition relations for phases in petrological calculations: an asymmetric multicomponent formulation. *Contributions to Mineralogy and Petrology*, **145,** 492–501.
Holland, T.J.B., Baker, J. & Powell, R., 1998. Mixing properties and activity-composition relationships of chlorites in the system MgO-FeO-Al_2O_3-SiO_2-H_2O. *European Journal of Mineralogy*, **10,** 395–406.
John, T., Scherer, E.E., Schenk, V., Herms, P., Halama, R. & Garbe-Schonberg, D., 2010. Subducted seamounts in an eclogite-facies phiolite sequence: the Andean Raspas Complex, SW Ecuador. *Contributions to Mineralogy and Petrology*, **159,** 265–284.
Kabir, M.F. & Takasu, A., 2010. Evidence for multiple burial-partial exhumation cycles from the Onodani eclogites in the Sambagawa metamorphic belt, central Shikoku, Japan. *Journal of Metamorphic Geology*, **28,** 873–893.
Karason, H. & van der Hilst, R.D., 2000. Constraints on mantle convection from seismic tomography. In: *The History and Dynamics of Global Plate Motion*. (eds Richards, M.R., Gordon, R. & van der Hilst, R.D.), pp. 277–288. Washington, DC, vol. **121**, AGU Geophys. Monogr.
van Keken, P.E., Hacker, B.R., Syracuse, E.M. & Abers, G.A., 2011. Subduction factory: 4. Depth-dependent flux of H_2O from subducting slabs worldwide. *Journal of Geophysical Research*, **116,** B01401. doi:10.1029/2010JB007922.
Kirby, S.H., 2000. Taking the temperature of slabs. *Nature*, **403,** 31–34.
Klemd, R., John, T., Scherer, E.E., Rondenay, S. & Gao, J., 2011. Changes in dip of subducted slabs at depth: petrological and geochronological evidence from HP-UHP rocks (Tianshan, NW-China). *Earth and Planetary Science Letters*, **310,** 9–20.
Krebs, M., Maresch, W.V., Schertl, H.P. *et al*., 2008. The dynamics of intra-oceanic subduction zones: a direct comparison between fossil petrological evidence (Rio San Juan Complex, Dominican Republic) and numerical simulation. *Lithos*, **103,** 106–137.
Litasov, K.D. & Ohtani, E., 2005. Phase relations in hydrous MORB at 18–28 GPa: implications for heterogeneity of the lower mantle. *Physics of the Earth and Planetary Interiors*, **150,** 239–263.
Lü, Z., Zhang, L.F., Du, J.X. & Bucher, K., 2008. Coesite inclusions in garnet from eclogitic rocks in western Tianshan, northwest China: convincing proof of UHP metamorphism. *American Mineralogist*, **93,** 1845–1850.
Lü, Z., Zhag, L.F., Du, J. & Bucher, K., 2009. Petrology of coesite-bearing ecloite from Habutengsu Valley, western Tianshan, NW China and its tectonometamorphic implication. *Journal of Metamorphic Geology*, **27,** 773–787.
Malatesta, C., Gerya, T., Scambelluri, M., Federico, L., Crispini, L. & Capponi, G., 2012. Intraoceanic subduction of 'heterogeneous' oceanic lithosphere in narrow basins: 2D numerical modeling. *Lithos*, **140–141,** 234–251.
Manning, C.E., 2004. The chemistry of subduction-zone fluids. *Earth and Planetary Science Letters*, **223,** 1–16.
Marmo, B.A., Clarke, G.L. & Powell, R., 2002. Fractionation of bulk rock composition due to porphyroblast growth: effects on eclogite facies mineral equilibria, Pam Peninsula, New Caledonia. *Journal of Metamorphic Geology*, **20,** 151–165.
Miyazaki, K., Zulkarnain, I., Sopaheluwakan, J. & Wakita, K., 1996. Pressure–temperature conditions and retrograde paths of eclogites, garnet glaucophane rocks and schists from South Sulawesi, Indonesia. *Journal of Metamorphic Geology*, **14,** 549–563.
Och, D.J., Leitch, E.C., Caprarelli, G. & Watanabe, T., 2003. Blueschist and eclogite in tectonic mélange, Port Macquarie, New South Wales, Australia. *Mineralogical Magazine*, **67,** 609–624.
Okamoto, K. & Maruyama, S., 1999. The high-pressure synthesis of lawsonite in the MORB + H_2O system. *American Mineralogists*, **84,** 362–373.
Okay, A.I., Tüysüz, O., Satir, M. *et al*. , 2006. Cretaceous and Triassic subduction-accretion, high-pressure–low-temperature metamorphism, and continental growth in the Central Pontides, Turkey. *Geological Society of America Bulletin*, **118,** 1247–1269.
Parkinson, C.D., Miyazaki, K., Wakita, K., Barber, A.J. & Carswell, D.A., 1998. An overview and tectonic synthesis of the pre-tertiary very-high-pressure metamorphic and associated rocks of Java, Sulawesi and Kalimantan, Indonesia. *The Island Arc*, **7,** 184–200.
Peacock, S.M. & Wang, K., 1999. Seismic consequences of warm versus cool subduction metamorphism: examples from Southwest and Northeast Japan. *Science*, **286,** 937–939.
Perrillat, J.P., Ricolleau, A., Daniel, I. *et al*., 2006. Phase transformations of subducted basaltic crust in the upmost lower mantle. *Physics of the Earth and Planetary Interiors*, **157,** 139–149.
Platt, J.P., 1986. Dynamics of orogenic wedges and the uplift of high-pressure metamorphic rocks. *Geological Society of America Bulletin*, **97,** 1037–1053.
Plunder, A., Agard, P., Dubacq, B., Chopin, C. & Bellanger, M., 2012. How continuous and precise is the record of P-T paths? Insights from combined thermobarometry and thermodynamic modelling into subduction dynamics (Schistes Lustres, W. Alps). *Journal of Metamorphic Geology*, **30,** 323–346.
Poli, S., 1993. The amphibolite-eclogite transformation: an experimental stuffy on basalt. *American Journal of Science*, **293,** 1061–1107.
Powell, R. & Holland, T.J.B., 2008. On thermobarometry. *Journal of Metamorphic Geology*, **26,** 155–179.
Powell, R., Holland, T.J.B. & Worley, B., 1998. Calculating phase diagrams involving solid solutions via nonlinear equations, with examples using Thermocalc. *Journal of Metamorphic Geology*, **16,** 577–588.
Powell, R., Guiraud, M. & White, R.W., 2005. Truth and beauty in metamorphic mineral equilibria: conjugate variables and phase diagrams. *Canadian Mineralogists*, **43,** 21–33.
Rebay, G., Powell, R. & Diener, F.A., 2010. Calculated phase equilibria for a MORB composition in a P-T range, 450–650 °C and 18–28 kbar: the stability of eclogite. *Journal of Metamorphic Geology*, **28,** 635–645.
Saha, A., Basu, A.R., Wakabayashi, J. & Wortman, G.L., 2005. Geochemical evidence for a subducted infant arc in Franciscan high-grade-metamorphic tectonics blocks. *Geological Society of America Bulletin*, **117,** 1318–1335.

Schmidt, M.W. & Poli, S., 1998. Experimentally based water budgets for dehydrations slabs and consequences for arc magma generation. *Earth and Planetary Science Letters*, **163,** 361–379.

Schneider, J., Bosch, D., Monie, P. *et al.*, 2004. Origin and evolution of the Escambray Massif (Central Cuba): an example of HP/LT rocks exhumed during intraoceanic subduction. *Journal of Metamorphic Geology*, **22,** 227–247.

Schwartz, S., Allemand, P. & Guillot, S., 2001. Numerical model of the effect of serpentinites on the exhumation of eclogitic rocks: insights from the Monviso ophiolitic massif (Western Alps). *Tectonophysics*, **342,** 193–206.

Shibakusa, H. & Maekawa, H., 1997. Lawsonite-bearing eclogitic metabasites in the Cazadero area, northern California. *Mineralogy and Petrology*, **61,** 163–180.

Shreve, R.L. & Cloos, M., 1986. Dynamics of sediment subduction, mélange formation, and prism accretion. *Journal of Geophysical Research*, **91,** 10229–10245.

Song, S., Zhang, L., Niu, Y., Su, L., Song, B. & Liu, D., 2006. Evolution from oceanic subduction to continental collision: a case study from the Northern Tibetan Plateau based on geochemical and geochronological data. *Journal of Petrology*, **47,** 435–455.

Spandler, C., Pettke, T. & Rubatto, D., 2011. Internal and external fluid source for eclogite-facies veins in the Monviso meta-ophiolite, Western Alps: implications for fluid flow in subduction zones. *Journal of Petrology*, **52,** 1207–1236.

Stanek, K.P., Maresch, W.V., Grafe, F., Grevel, C.H. & Baumann, A., 2006. Structure, tectonic and metamorphic development of the Sancti Spirtus Dome (eastern Escambray massif, Central Cuba). *Geological Acta*, **4,** 151–170.

Štípská, P., Schulmann, K., Lehmann, J., Corsini, M., Lexa, O. & Tomurhuu, D., 2010. Early Cambrian eclogites in SW Mongolia: evidence that the Palaeo-Asian Ocean suture extends further east than expected. *Journal of Metamorphic Geology*, **28,** 915–933.

Syracuse, E.M., van Keken, P.E. & Abers, G.A., 2010. The global range of subduction zone thermal models. *Physics of the Earth and Planetary Interiors*, **51,** 1761–1782.

Tsujimori, T. & Matsumoto, K., 2006. P-T pseudosection of a glaucophane-epidote eclogite from Omi serpentinite melange, SW Japan: a preliminary report. *Journal of the Geological Society of Japan*, **112,** 407–414.

Tsujimori, T., Sisson, V.B., Liou, J.G., Harlow, G.E. & Sorensen, S.S., 2006a. Petrologic characterization of Guatemalan lawsonite eclogite: eclogitization of subducted oceanic crust in a cold subduction zone. The Geological Society of America Special Paper, **403,** 147–168.

Tsujimori, T., Sisson, V.B., Liou, J.G., Harlow, G.E. & Sorensen, S.S., 2006b. Very-low-temperature record of the subduction process: a review of worldwide lawsonite eclogites. *Lithos*, **92,** 609–624.

Tsujimori, T., Matsumoto, K., Wakabayashi, J. & Liou, J.G., 2006c. Franciscan eclogite revisited: reevalueation of the P-T evolution of tectonic blocks from Tiburon Peninsula, California, USA. *Mineralogy and Petrology*, **88,** 243–267.

Usui, T., Nakamura, E., Kobayashi, K., Maruyama, S. & Helmstaedt, H., 2003. Fate of the subducted Farallon plate inferred from eclogite xenoliths in the Colorado Plateau. *Geology*, **31,** 589–592.

Usui, T., Nakamura, E. & Helmstaedt, H., 2006. Petrology and geochemistry of eclogite xenoliths from the Colorado Plateau: implications for the evolution of subducted crust. *Journal of Petrology*, **47,** 929–964.

Vignaroli, G., Rossetti, F., Bouybaouene, M., *et al.*, 2005. A counter-clockwise *P–T* path for the Voltri Massif eclogites (Ligurian Alps, Italy). *Journal of Metamorphic Geology*, **23,** 533–555.

Wallis, S., Takasu, A., Enami, M. & Tsujimori, T., 2000. A re-evaluation of eclogite facies metamorphism in SW Japan: proposal for an eclogite nappe. *Journal of Metamorphic Geology*, **18,** 653–664.

Wei, C.J. & Clarke, G.L., 2011. Calculated phase equilibria for MORB compositions: a reappraisal of the metamorphic evolution of lawsonite eclogite. *Journal of Metamorphic Geology*, **29,** 939–952.

Wei, C.J. & Song, S.G., 2008. Chloritoid–glaucophane schist in the north Qilian orogen, NW China: phase equilibria and P-T path from garnet zonation. *Journal of Metamorphic Geology*, **26,** 301–316.

Wei, C.J., Yang, Y., Su, X.L., Song, S.G. & Zhang, L.F., 2009a. Metamorphic evolution of low-T eclogite from the North Qilian orogen, NW China: evidence from petrology and calculated phase equilibria in the system NCKFMASHO. *Journal of Metamorphic Geology*, **27,** 55–70.

Wei, C.J., Wang, W., Clarke, G., Zhang, L.F. & Song, S.G., 2009b. Metamorphism of high/ultra high-pressure pelitic – felsic Schist in the South Tianshan Orogen, NW China: phase equilibria and P-T path. *Journal of Petrology*, **50,** 1973–1991.

White, R.W., Powell, R. & Holland, T.J.B., 2007. Progress relating to calculation of partial melting equilibria for metapelites and felsic gneisses. *Journal of Metamorphic Geology*, **25,** 511–527.

White, R.W., Stevens, G. & Johnson, T.E., 2011. Is the crucible reproducible? Reconciling melting experiments with thermodynamic calculations. *Elements*, **7,** 241–246.

Wu, Y., Fei, Y.W., Jin, Z.M. & Liu, X.Y., 2009. The fate of subducted upper continental crust: an experimental study. *Earth and Planetary Science Letters*, **282,** 275–284.

Zack, T., Rivers, T., Brumm, R. & Kronz, A., 2004. Cold subduction of oceanic crust: implications from a lawsonite eclogite from the Dominican Republic. *European Journal of Mineralogy*, **16,** 909–916.

Zhai, Q.G., Zhang, R.Y., Jahn, B-.M., Li, C., Song, S.G. & Wang, J., 2011. Triassic eclogites from central Qiangtang, northern Tibet, China: petrology, geochronology and metamorphic *P–T* path. *Lithos*, **125,** 173–189.

Zhang, L.F., Lü, Z. & Song, S.G., 2008. The geological characteristic of oceanic-type UHP metamorphic belts and their tectonic implications: case studies from Southwest Tianshan and North Qaidan in NW China. *Chinese Science Bulletin*, **53,** 3120–3130.

Zhao, D.P., 2008. Multiscale seismic tomography and mantle dynamics. *Gondwana Research*, **15,** 297–323.

Zhao, D.P., Maruyama, S. & Omori, S., 2007. Mantle dynamics of western Pacific to East Asia: new insight from seismic tomography and mineral physics. *Gondwana Research*, **11,** 120–131.

Zhao, Z., Niu, Y., Christensen, N.I. *et al.*, 2011. Delamination and ultra-deep subduction of continental crust: constraints from elastic wave velocity and density measurement in ultrahigh-pressure metamorphic rocks. *Journal of Metamorphic Geology*, **29,** 781–801.

Received 3 September 2012; revision accepted 11 February 2013.